Southern Ocean Deep Circulation and Heat Uptake in a High-Resolution Climate Model

EMILY R. NEWSOM

Department of Earth and Space Sciences, University of Washington, Seattle, Washington

CECILIA M. BITZ

Department of Atmospheric Sciences, University of Washington, Seattle, Washington

FRANK O. BRYAN

Climate and Global Dynamics Division, National Center for Atmospheric Research, Boulder, Colorado

RYAN ABERNATHEY

Department of Earth and Environmental Sciences, Columbia University, New York, New York

PETER R. GENT

Climate and Global Dynamics Division, National Center for Atmospheric Research, Boulder, Colorado

(Manuscript received 23 July 2015, in final form 20 January 2016)

ABSTRACT

The dynamics of the lower cell of the meridional overturning circulation (MOC) in the Southern Ocean are compared in two versions of a global climate model: one with high-resolution (0.1°) ocean and sea ice and the other a lower-resolution (1.0°) counterpart. In the high-resolution version, the lower cell circulation is stronger and extends farther northward into the abyssal ocean. Using the water-mass-transformation framework, it is shown that the differences in the lower cell circulation between resolutions are explained by greater rates of surface water-mass transformation within the higher-resolution Antarctic sea ice pack and by differences in diapycnal-mixing-induced transformation in the abyssal ocean.

While both surface and interior transformation processes work in tandem to sustain the lower cell in the control climate, the circulation is far more sensitive to changes in surface transformation in response to atmospheric warming from raising carbon dioxide levels. The substantial reduction in overturning is primarily attributed to reduced surface heat loss. At high resolution, the circulation slows more dramatically, with an anomaly that reaches deeper into the abyssal ocean and alters the distribution of Southern Ocean warming. The resolution dependence of associated heat uptake is particularly pronounced in the abyssal ocean (below 4000 m), where the higher-resolution version of the model warms 4.5 times more than its lower-resolution counterpart.

1. Introduction

The vast majority of the energy gained by the climate system during periods of global radiative imbalance is stored within the global ocean (e.g., Levitus et al. 2001;

Corresponding author address: Emily R. Newsom, Department of Earth and Space Sciences, University of Washington, Johnson Hall Rm. 070, Box 351310, 4000 15th Avenue NE, Seattle, WA 98195-1310.
E-mail: enewsom@uw.edu

Abraham et al. 2013). The effective volume of ocean available to warm at a given time is set by the rate at which heat can be moved from the surface mixed layer into the deep ocean (e.g., Hansen et al. 1985), redirecting heat that would otherwise warm the surface. Therefore, deep ocean heat uptake plays a critical role in slowing the pace of global surface warming in response to greenhouse gas forcing (e.g., Gregory 2000; Held et al. 2010; Raper et al. 2002; Kostov et al. 2014).

The deep and abyssal ocean is filled by water masses formed at the high latitudes; deep ocean heat uptake

proceeds through the warming and redistribution of these polar-sourced water masses. The deep water mass formed at the Southern Ocean surface, Antarctic Bottom Water (AABW), comprises a large fraction of the oldest waters found in the global abyssal ocean (Johnson 2008; Gebbie and Huybers 2012). Consequently, the heat content of the global abyssal ocean is directly influenced by Southern Ocean processes. Indeed, the estimated $0.1\,\mathrm{W\,m^{-2}}$ rate of global ocean heat uptake below 2000 m over the last 30 years was primarily driven by the warming of AABW. This warming is likely linked to changes in the surface ocean and climate around Antarctica (Purkey and Johnson 2010, 2013). Further, the impact of ocean heat uptake is particularly high within the Southern Ocean, where it acts to curb surface warming that would otherwise be strongly amplified by the combined effects of the sea ice–albedo feedback and a stably stratified atmosphere (Armour et al. 2013).

While the Southern Ocean plays a fundamental role in climate change, the unique influence of small-scale processes on its circulation presents modeling challenges. Processes such as mesoscale eddy mixing, internal wave breaking, turbulent overflows, and convection have first-order effects on the overturning circulation. Because these processes are often subgrid scale in modern general circulation models (GCMs), they are either parameterized or underresolved. The simplest and most ubiquitous parameterization is grid-scale diffusion and viscosity, which is often prescribed by numerical considerations rather than physical ones. Deep ocean circulation and stratification are quite sensitive to diapycnal diffusion (Bryan 1987; Cummins et al. 1990), and diffusion (including spurious numerical diffusion) is itself resolution dependent (Griffies et al. 2000; Hill et al. 2012; Urakawa and Hasumi 2014). Coarse-resolution models employ mesoscale eddy transport schemes, composed of isopycnal diffusion (Redi 1982) and eddy-induced advection (Gent and McWilliams 1990, hereafter GM). These parameterizations involve tuning parameters that strongly influence the circulation (Danabasoglu and McWilliams 1995; Gnanadesikan 1999; Pradal and Gnanadesikan 2014; Gnanadesikan et al. 2015). Overflow parameterizations have been employed with limited success (Danabasoglu et al. 2012; Snow et al. 2015), as have abyssal tidal mixing schemes (Jayne 2009). The recent advent of global mesoscale resolving/permitting ocean models allows some such parameterizations and other scale-dependent processes to be evaluated against more direct explicit simulation, especially with respect to the mesoscale (McClean et al. 2011; Griffies et al. 2015).

The potential for inadequate model resolution to bias Southern Ocean dynamics has garnered substantial attention in the literature. The focus has been mostly directed toward the behavior of the upper cell of the meridional overturning circulation (MOC) (see, e.g., Henning and Vallis 2005; Hallberg and Gnanadesikan 2006; Farneti et al. 2010; Abernathey et al. 2011; Gent and Danabasoglu 2011; Bryan et al. 2014; Farneti et al. 2014; Gent 2016). In contrast, the impact of model resolution on the lower cell of the MOC and its relationship to Southern Ocean abyssal heat uptake is relatively unexplored. This is the aim of our paper.

The lower MOC is sustained by processes that make surface water denser, "pushing" water into the abyssal ocean, and processes that reduce the density of dense water in the interior, "pulling" it upward again. In the abyssal ocean, water is pulled up via diapycnal mixing, the magnitude of which is likely a key control on abyssal overturning strength (Nikurashin and Vallis 2011, 2012). Such mixing is accomplished by the breaking of locally generated internal waves over bathymetric features, geothermal heating, remote tidal dissipation, and entrainment across strong density gradients in localized overflows (Naveira Garabato et al. 2004, 2007; Nikurashin et al. 2012; de Lavergne et al. 2016). Transient eddy fluxes, which redistribute potential energy and result in the northward transport of dense water in the abyss, have also been linked to mixing rates and overturning strength because of their influence on abyssal stratification (Ito and Marshall 2008). A misrepresentation of these abyssal diapycnal mixing processes could introduce biases into the lower cell dynamics.

The descending branch of the lower cell is sustained by buoyancy loss at high latitudes via the interaction of cold, salty water rejected during sea ice growth (especially in coastal polynyas and leads); extremely cold, fresh water formed from sub-ice-shelf melting; and comparatively warm, salty Lower Circumpolar Deep Water (LCDW) that upwells near the coast (Orsi et al. 1999; Jacobs 2004; Gordon 2001). Polynyas and leads, which are key moderators of heat loss and brine rejection, form on spatial and temporal scales below the resolution of the current generation of GCMs (Stössel et al. 2007; Willmott et al. 2007). Additionally, recent studies have suggested that transient eddies are key to the transport of AABW across the continental shelf front [where the deformation radius is $O(1–10)$ km], as is the input of momentum from coastal easterly winds (Stewart and Thompson 2012, 2015a; Thompson et al. 2014). In sum, sea ice formation, the formation of dense plumes, transient cross-shelf flow, and sub-ice-shelf processes all occur on scales smaller than the grid spacing of most GCMs; as a result, most models misrepresent the volume and formation rate of AABW. Indeed, Heuzé et al. (2013) found that no model participating in phase 5

of the Coupled Model Intercomparison Project (CMIP5; Taylor et al. 2012) formed AABW via the sinking of shelf waters. Instead the majority of models formed bottom waters by (possibly spurious) open-ocean convection, leading to large biases in the abyssal ocean density simulated in most of the CMIP5 models analyzed in their study.

Here, we explore how increasing model resolution in the ocean and sea ice components influences the dynamics of the lower cell of the MOC. We are motivated by the following questions: Does resolution alter the lower cell in the mean state? And does resolution affect the rate of Southern Ocean heat uptake under greenhouse warming? Ours is the first study to investigate the resolution dependence of this circulation in a coupled model, to the best of our knowledge. We use a GCM configured at resolution high enough to capture coastal polynyas and to explicitly resolve transient eddies throughout much of the global ocean and compare the results to a lower-resolution counterpart, configured at a resolution typical of CMIP5 models.

2. Model setup and analysis

a. Model and experiments

We use the Community Climate System Model, version 3.5 (CCSM3.5), with ocean and sea ice at two resolutions, while maintaining identically configured atmosphere and land components. The high-resolution version (HR) is run with 0.1° resolution in the sea ice and ocean components. The comparatively low-resolution version (LR) is run at 1° resolution in the ocean and sea ice. The atmospheric component has a finite-volume dynamical core and is run in both cases at identical resolution: 26 vertical levels, with horizontal resolution of 0.47° × 0.63° (as in Gent et al. 2010). The horizontal resolution of the land model is the same as for the atmosphere. The HR and LR setups are identical to those used in Kirtman et al. (2012), Bitz and Polvani (2012), and Bryan et al. (2014).

HR has a sufficiently fine ocean horizontal grid to be deemed eddy resolving at low and midlatitudes and eddy permitting at very high latitudes (south of ~50°S), following Smith et al. (2000). Grid spacing near the Antarctic coast is ~3–5 km, which we will show improves the resolution of sea ice dynamics. In contrast, LR is non–eddy resolving and relies on the GM eddy parameterization with a spatially and temporally varying GM coefficient that depends on the square of the local buoyancy frequency [see Danabasoglu and Marshall (2007) and Gent and Danabasoglu (2011)]. No overflow

parameterizations were employed in this model, and neither of the resolutions examined here exhibits grid-scale-size, full-depth open-ocean convection [a problem endemic to some GCMs (i.e., Heuzé et al. 2013)]. Control integrations of HR and LR were run with 1990s carbon dioxide mixing ratios for 167 yr. Kirtman et al. (2012) describe in depth the configuration and climate of the control integrations.

Perturbed runs were branched from the control integrations of each resolution (LR and HR) at year 77. Each perturbed run was subject to a 1% increase in the carbon dioxide mixing ratio of the atmosphere until carbon dioxide doubling was reached at year 147; thereafter, carbon dioxide mixing ratios were held fixed for the next 20 yr. To minimize the impact of possible climate drift, we define the "response" or "anomaly" of a given field in a perturbed run as the difference between its average during the 20-yr period after carbon dioxide doubling and its average during the contemporaneous 20 yr in the control integration. Because of the computational expense at high resolution, our control runs are necessarily short relative to the equilibration time scale of the deep ocean, and there is still a small drift in deep ocean temperatures from the branch point to the end of the control runs at either resolution (see Kirtman et al. 2012). We find this drift has a minimal effect on isopycnal inflation (explained subsequently) in our control simulations. However, we cannot conclusively rule out that the features we diagnose are transient.

One limitation of this model, of particular relevance to this study, is the absence of interactive ice shelves. Instead, the mass balance of Antarctica is enforced by uniformly freshening and cooling the ocean at the continental margin by any precipitation reaching the Antarctic continent that causes the snow depth to exceed a maximum value of 1 m, termed "ice runoff." Raising carbon dioxide results in an increase in ice runoff owing to higher snowfall rates over Antarctica from increased poleward moisture transport. However, in this model, the reduction in sea ice formation and increase in precipitation over the ocean near Antarctica are a much greater source of anomalous freshwater than Antarctic ice or meltwater runoff (see Kirkman and Bitz 2011).

b. Isopycnal overturning and water-mass transformation

A challenge to understanding the impact of model resolution on circulation is the certainty that increasing resolution will affect multiple processes simultaneously. We try to assess how different processes alter the circulation by employing the water-mass-transformation

framework, first introduced by Walin (1982) and further developed in many subsequent studies (e.g., Speer and Tziperman 1992; Marsh et al. 2000; Bryan et al. 2006; Iudicone et al. 2008). We consider the ocean circulation most directly related to stratification by calculating an overturning streamfunction along surfaces of constant density (Döös and Webb 1994). We refer to the time average of this field

$$\psi^{\sigma}(\sigma, y) \equiv -\frac{1}{(t_1 - t_0)} \int_{t_0}^{t_1} \int_{x_W}^{x_E} \int_{-B(x,y)}^{z(x,y,\sigma,t)} v(x, y, z, t) \, dz \, dx \, dt$$

(1)

as the isopycnal MOC, where v is the total meridional velocity (including the bolus velocity in LR), σ is potential density, x is longitude (positive eastward), y is latitude (positive northward), z is depth (positive upward), B is the ocean bottom depth, and t is time. The component of the MOC from Eq. (1) with v equal to the time-mean velocity and σ equal to the time-mean isopycnal depth is the mean isopycnal MOC, ψ_m^{σ}. The impact of transient eddies on the isopycnal MOC (or the transient eddy-induced isopycnal MOC, ψ_E^{σ}) can be expressed as the difference between the total and mean MOC components:

$$\psi_E^{\sigma} = \psi^{\sigma} - \psi_m^{\sigma}.$$

(2)

The transient eddy-induced MOC emerges as a result of explicitly resolved eddies in HR, while in LR it is computed from the GM-parameterized bolus velocity field using Eq. (1) with $v = v_{bolus}$. At either resolution, the impact of standing eddies and gyres as well as any steady correlations between density and zonally nonuniform flow can be expressed as the difference between the mean isopycnal MOC and a depth–space MOC, ψ^z (Dufour et al. 2012), the latter of which is calculated in the more traditional method relative to surfaces of constant depth.

The isopycnal circulation ψ^{σ} persists on a global scale because of the continual redistribution of seawater between density classes. As illustrated in Fig. 1, the volume of a region of the ocean V, below and southward of isopycnal σ and latitude y, varies with the volume flux across its boundaries. Considering the volume V south of any given σ and y, the volume inflation can be expressed as

$$\frac{d}{dt} V(\sigma, y, t) = \psi^{\sigma}(\sigma, y, t) - [F(\sigma, y, t) + \text{Dmix}(\sigma, y, t)],$$

(3)

where the latter two terms together represent water-mass transformation, with $F(\sigma, y, t)$ induced by air–sea fluxes at the sea surface (surface transformation) and
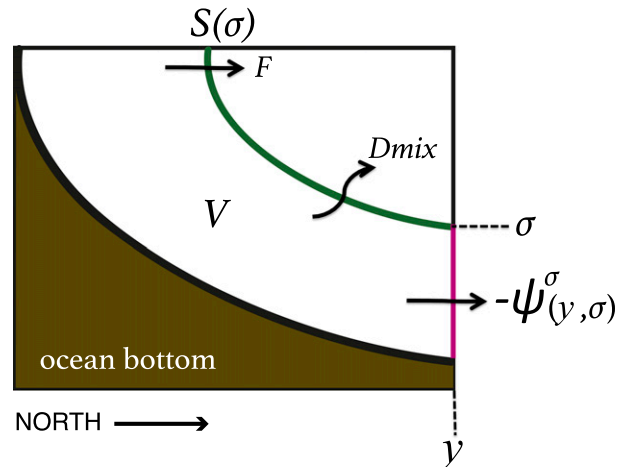

FIG. 1. Schematic to demonstrate processes controlling the volume V poleward of an isopycnal surface σ and latitude y in Eq. (3). Volume fluxes into V include contributions of surface transformation induced by surface fluxes south of the outcrop at $S(\sigma)$ (component F), contributions from diapycnal mixing across the isopycnal surface σ (component Dmix), and total southward flow across y and below σ (component ψ^{σ}). Colors are added to the lines denoting the isopycnal surface (green), ocean surface (black), and latitude transect (pink) to orient the reader to the components of diapycnal volume flux illustrated in Figs. 6 and 13.

Dmix(σ, y, t) induced by mixing across density surfaces in the interior (interior transformation). A general definition of surface transformation F_{gen} is

$$F_{gen}(\sigma, t) = -\frac{\partial}{\partial \sigma} \iint_{A[\sigma^* > \sigma]} f_{surf}(x, y, t) \, dA,$$

(4)

where f_{surf} is the spatial distribution of surface density flux, a function of heat and freshwater fluxes (f_{heat} and f_{water}, defined positive downward):

$$f_{surf}(x, y, t) = -\frac{\alpha}{c_p} f_{heat}(x, y, t) - \frac{\rho_o}{\rho_{fw}} \beta S_o f_{water}(x, y, t).$$

(5)

Here, α and β are the coefficients of thermal expansion and saline contraction, respectively, c_p is the specific heat of seawater, ρ_o is a reference seawater density, ρ_{fw} is the density of freshwater, and S_o is a reference salinity. To directly compare surface transformation to the circulation at a given latitude y, as in Eq. (3), we must consider only the net surface transformation occurring south of y, which we call simply F. This can be calculated as

$$F(\sigma, y, t) = F_{gen}(\sigma, t)\mathcal{H}[\sigma - \sigma_{min}(y, t)],$$

(6)

where $\mathcal{H}$ is the Heaviside function and σ_{min} is the lowest density to outcrop at latitude y. The flux F is positive toward lighter densities for direct comparison with the

MOC in the Southern Hemisphere. The interior transformation Dmix can be defined similarly to F; however, doing so requires knowledge of time-varying, three-dimensional diffusive fluxes, which were not saved for these simulations because of data storage limitations. Instead, we follow Marsh et al. (2000) and calculate Dmix at latitude y as a residual of the other terms in Eq. (3). This effectively measures the path integrated interior transformation at each density between the surface and y. With this method, we cannot identify the specific mixing processes responsible for interior diapycnal volume fluxes, though we can gain insight into the relative importance of surface and interior transformation on MOC strength.

It is important to note two caveats to our analysis. First, we use a reference pressure of 2000 dbar (1 dbar = 10^4 Pa) to calculate potential density, known as σ_2, for both our surface transformation and MOC calculations, since our focus is on the deep ocean; however, the choice of reference pressure may affect our results (Iudicone et al. 2008; Stewart and Thompson 2015b). Second, because of prohibitive amounts of data generated in HR, we were restricted to saving monthly data, meaning that higher-frequency transient behavior is not captured in our analysis. Ballarotta et al. (2013) explored the temporal and spatial scales at which transient behavior was most influential: though daily time scales were important to the upper MOC cell, their impact was much smaller in the lower MOC cell. Furthermore, in a spectral analysis of eddy heat fluxes in the same class of eddy-resolving model, Abernathey and Wortham (2015) found that submonthly variability makes a negligible contribution to the total heat flux. Thus, we expect to capture the majority of transient fluctuations most relevant for our analysis.

3. Control state results

It is essential to understand the mean state of the Southern Ocean at each resolution to interpret how resolution affects the response to carbon dioxide forcing. Compared to LR, HR produces consistently saltier and colder waters on the continental shelf and throughout the deep Southern Ocean (Figs. 2a–f). In the abyssal ocean (below 4000 m) waters are colder by approximately 0.45°C and saltier by approximately 0.016 psu on average. Near the surface, HR forms a fresher branch of Antarctic Intermediate Water (AAIW) and warmer surface water. In comparison to World Ocean Circulation Experiment (WOCE: publically available at http://cchdo.ucsd.edu) hydrographic data, both model resolutions form deep waters that are too saline. This salinity bias is more pronounced in HR,

which may be the result of nonlocal processes impacting the salinity of upwelling Circumpolar Deep Water (CDW), such as by brine rejection from sea ice in the Northern Hemisphere (Kirtman et al. 2012). Bottom waters formed in HR are too cold in some regions, while bottom waters in LR are consistently too warm. An example of these large-scale properties is shown along an Indian Ocean transect [WOCE identification Indian Ocean line 8 (IO8) in Figs. 2g–l], though we note that the comparison between each model and observations varies significantly with region.

These zonally averaged properties arise from rich spatial structures. Irrespective of resolution, the densest waters in the abyssal ocean (Figs. 3c,d) outcrop in the coastal regions of the Ross and Weddell Seas (Figs. 3a,b). The waters extending from the high-latitude surface into the abyssal ocean are notably denser in HR. The densest of these bottom waters emanate from the Ross and Weddell continental shelves, as is illustrated by the distribution of ocean bottom temperature and salinity (Fig. 4). Both the density and the density response to increased resolution are highest in these shelf regions, and both decrease with distance from the shelf following topographically driven AABW export pathways. These distributions imply that differences in surface properties propagate into the deep ocean from these locations.

To understand how differences in stratification and abyssal properties are manifested in the large-scale circulation, we examine the MOC south of the equator. In Fig. 5, we show the relative contributions toward the circulation ψ^σ from each of the components in Eq. (2). In our control simulation, the volume inflation contributes only a small term [on the order of 1 Sverdrup (Sv; 1 Sv $\equiv$ 10^6 m^3 s^{-1})], and thus we ignore it in this calculation. To visualize the spatial distribution of the large-scale isopycnal circulation, we have projected each component onto the depth of each mean isopycnal in Fig. 5.

We focus our analysis on differences in the lower cell, which emerge more robustly when the circulation is defined along isopycnals (ψ^σ). In light of the recent focus on model resolution in the upper cell, as mentioned in the introduction, it is noteworthy that, in this model, features of the lower cell vary significantly with resolution. There are two distinct local minima in ψ^σ (see Figs. 5a–d). One minimum is associated with the export of dense surface waters into the abyssal ocean and their return flow, contained south of 55°S, which we define as the "subpolar range" of the lower cell. This feature is weak in the depth-space overturning, likely because much of the export of dense water occurs in the Ross and Weddell Gyres, as is suggested by the distribution of bottom temperature and salinity. The second minimum,
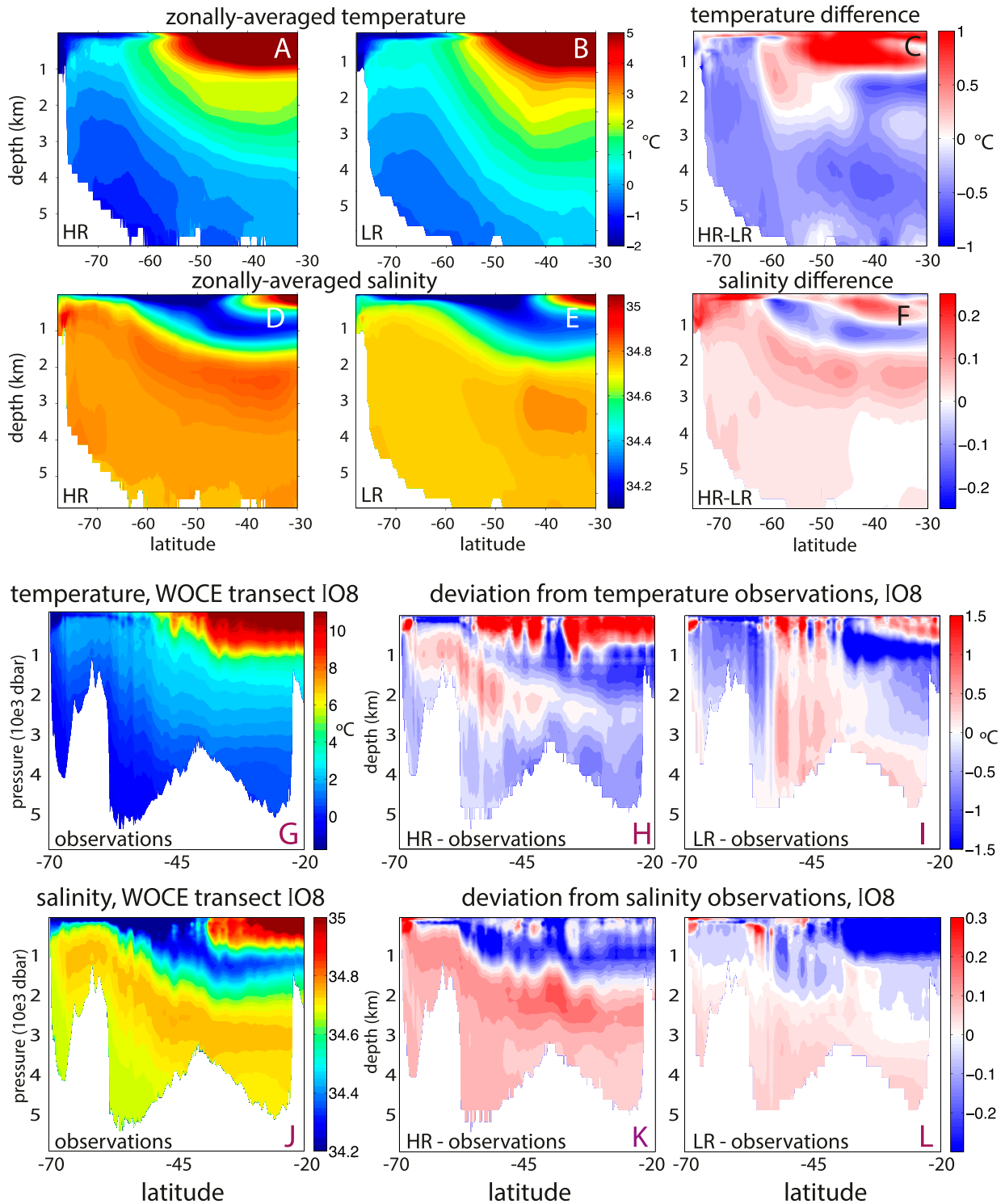
FIG. 2. Zonally averaged properties in the Southern Ocean for (a)–(c) potential temperature and (d)–(f) salinity in (a),(d) HR; (b),(e) LR; and (c),(f) HR minus LR. (g)–(i) Potential temperature and (j)–(l) salinity along the WOCE transect IO8 (longitude varies from 82° to 95°E) from (g),(j) observations; (h),(k) HR minus observations; and (i),(l) LR minus observations.
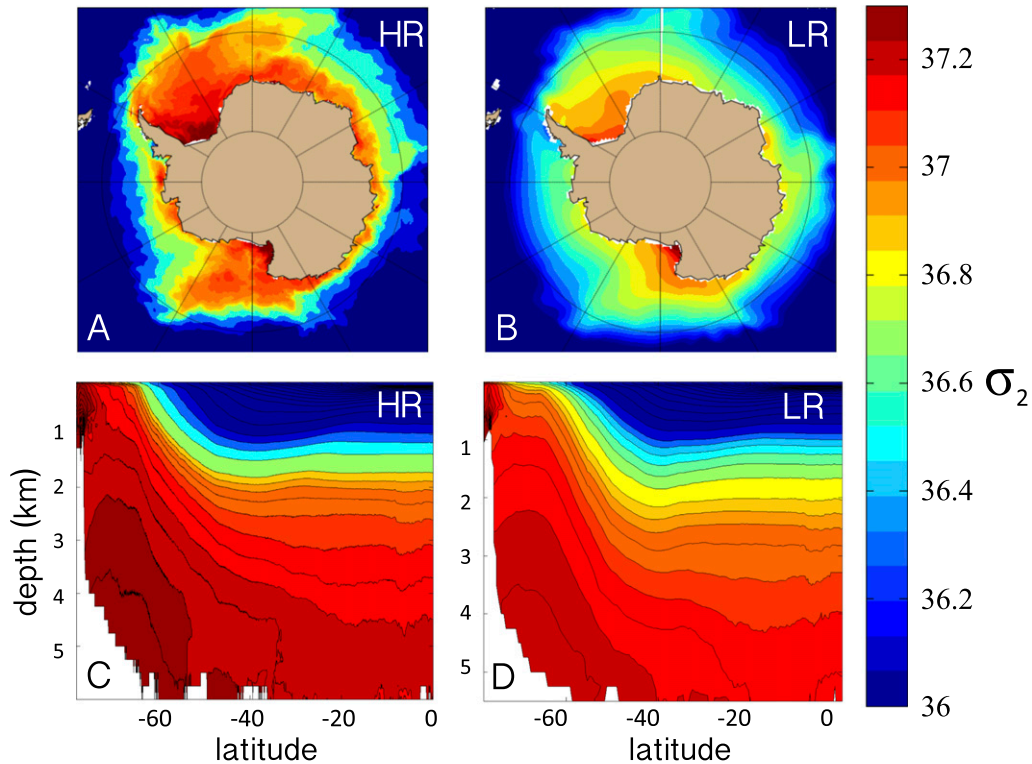
FIG. 3. Potential density referenced to 2000 dbar (σ_2) (kg m^{-3}). (a),(b) Annual-average surface σ_2 and (c),(d) annual-average, zonal-average σ_2 in (a),(c) HR and (b),(d) LR. Color scale is chosen to highlight density variations in the deep and polar surface ocean.

in what we refer to as the "abyssal range" of the lower cell to describe overturning north of 55°S and south of the equator, is associated with the circulation of dense waters north of the Antarctic Circumpolar Current (ACC). Across this latitude range, bottom waters must mix sufficiently with lighter waters to upwell at the polar surface. The apparent spatial separation of these circulation minima, seen in most climate models (Farneti et al. 2015), derives from the partial recirculation of Weddell and Ross Sea waters at high latitudes. This separation is much reduced by density transport achieved by eddy fluctuations (resolved or parameterized), evident in the transient eddy-induced stream-functions shown in Fig. 5. This counterclockwise transient eddy-induced cell, ψ_E^σ, is strongest between 45° and 60°S and reaches from the upper ocean to the full depth (Figs. 5e,f). The lack of resolution dependence in the structure of ψ_E^σ suggests that the eddy parameterization in LR is well calibrated, though ψ_E^σ is stronger near the ocean bottom in HR, indicating that resolved eddies may alter the northward export of very dense AABW. Further, it is possible that we underestimate the strength of the HR eddy-induced cell by using monthly velocities in Eq. (1), particularly in the upper cell, where

daily correlations between velocity and temperature may become more important (Ballarotta et al. 2013).

In contrast to ψ_E^σ, there are striking resolution-dependent differences in the mean isopycnal overturning ψ_m^σ (Fig. 5c vs Fig. 5d); these differences dominate the resolution dependence of the total overturning ψ^σ. Mean transport in the subpolar range is stronger in HR (26 Sv vs 22 Sv in LR) and occurs on isopycnals that are deeper in the zonal average, corresponding to the production of more and relatively denser AABW in HR, consistent with the abyssal temperature and salinity fields. Mean overturning in the abyssal range extends farther northward and remains stronger throughout the abyssal ocean in HR, with an overturning maximum of 20 Sv around 40°S. In contrast, the majority of lower cell overturning occurs south of 50°S in LR, north of which abyssal overturning becomes relatively weak (with a maximum of 6 Sv).

The influence of resolution on surface and interior processes driving diapycnal volume exchange can be compared via Eq. (3). Implicit to this analysis is the notion that both surface fluxes and interior mixing processes can change the density of seawater on a given isopycnal, and, in turn, any change in density must
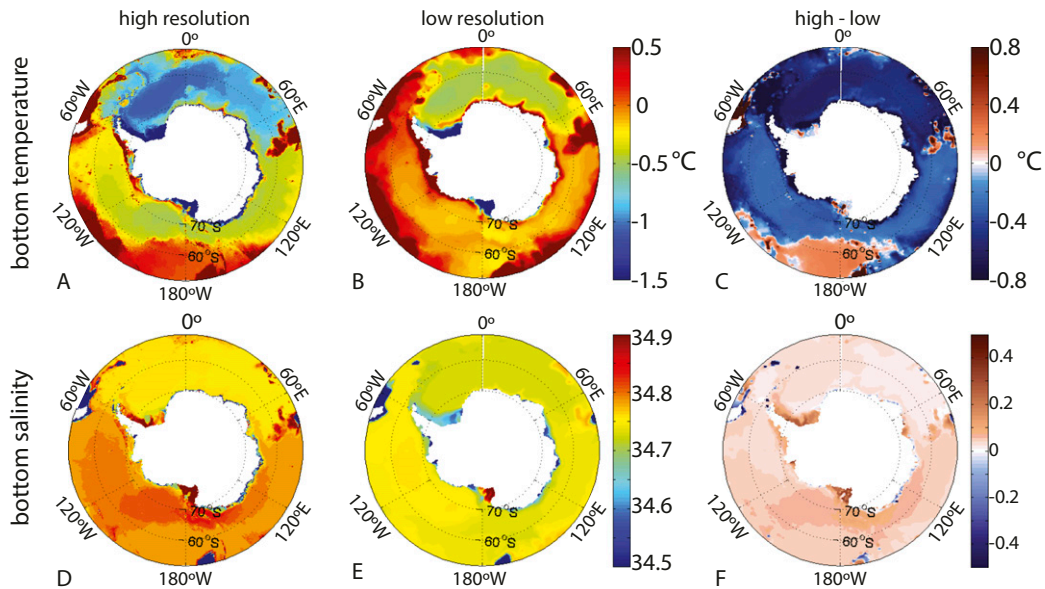
FIG. 4. Ocean bottom properties south of 50°S for (a)–(c) temperature and (d)–(f) salinity in (a),(d) HR; (b),(e) LR; and (c),(d) HR minus LR. The ocean bottom is defined as the deepest ocean grid cell.

drive a volume flux of seawater across isopycnals; the transformation (separated into components F and Dmix) describes these induced volume fluxes. The sign of the transformation denotes the direction of this volume flux, where a positive transformation is a volume flux toward lighter isopycnals. Any slope in the transformation rate indicates that the diapycnal volume flux differs across neighboring isopycnals, thus inducing a convergence or divergence of seawater volume into or out of a given density class. In steady state, the convergence (divergence) of volume into a density class will necessitate export (import) of water at that density: that is, its formation (destruction).

The surface transformation function [$F(\sigma, y, t)$ in Eq. (3)] at 30°S captures the surface regeneration of the major water masses of the Southern Ocean: specifically, the regions of net positive transformation and net negative transformation associated with the upper cell and lower cell, respectively (see Fig. 6). Waters in the small density range of the lower cell (which differs slightly between models: $\sim 36.82 \leq \sigma \leq 37.72$ kg m^{-3} in HR and $\sim 36.20 \leq \sigma \leq 37.54$ kg m^{-3} in LR) occupies $\sim 70\%$ of the volume of the Southern Ocean; we focus our analysis on a shared density range that encompasses the majority of this cell at both resolutions ($\sigma_{\text{lower\_cell}}$, defined as $36.72 \leq \sigma \leq 37.72$ kg m^{-3}). Downwelling AABW is formed across the range of net volume flux convergence (≥ 37.25 kg m^{-3} in HR and ≥ 37.12 kg m^{-3} in LR), so transformation across this density range is of particular

importance to understanding what drives descent from the surface.

To diagnose the distribution of interior transformation Dmix, we consider how ψ^{σ} varies with density at a given latitude y_o. We then compare ψ^{σ} to the other terms in Eq. (3) (recalling that volume inflation is negligible) at several latitudes over the density range of the lower cell; the degree to which ψ^{σ} and F differ will indicate the impact diapycnal mixing has had on the circulation at each latitude. Figure 7 illustrates the relative strength of $\psi^{\sigma}(\sigma_{\text{lower\_cell}}, y_o)$, $F(\sigma_{\text{lower\_cell}}, y_o)$, and Dmix($\sigma_{\text{lower\_cell}}, y_o$) at $y_o = 64°$, 38°, and 30°S.

We first examine $y_o = 64°$S, chosen as a compromise between the northern extent of the Ross and Weddell shelves to capture how flow from the continental shelf into the abyssal ocean transforms water masses. Here, ψ^{σ} bears a close connection to F (Figs. 7a,b). Vigorous surface transformation leads to a peak in ψ^{σ} at $\sigma \sim 37.25$ kg m^{-3} in HR and $\sigma \sim 37.15$ kg m^{-3} in LR; this peak is modestly increased by the diapycnal mixing of very dense waters along their descent from the shelf into the abyss (i.e., Dmix drives a volume flux of 6 Sv in HR and 8 Sv in LR from the densest waters into the peak flow in ψ^{σ}). Somewhat surprisingly, the magnitude and relative distribution across density classes of this Dmix is similar between resolutions, though it is translated to slightly denser classes in HR because of the higher densities of waters formed at the surface. So, while a number of ocean processes may depend on
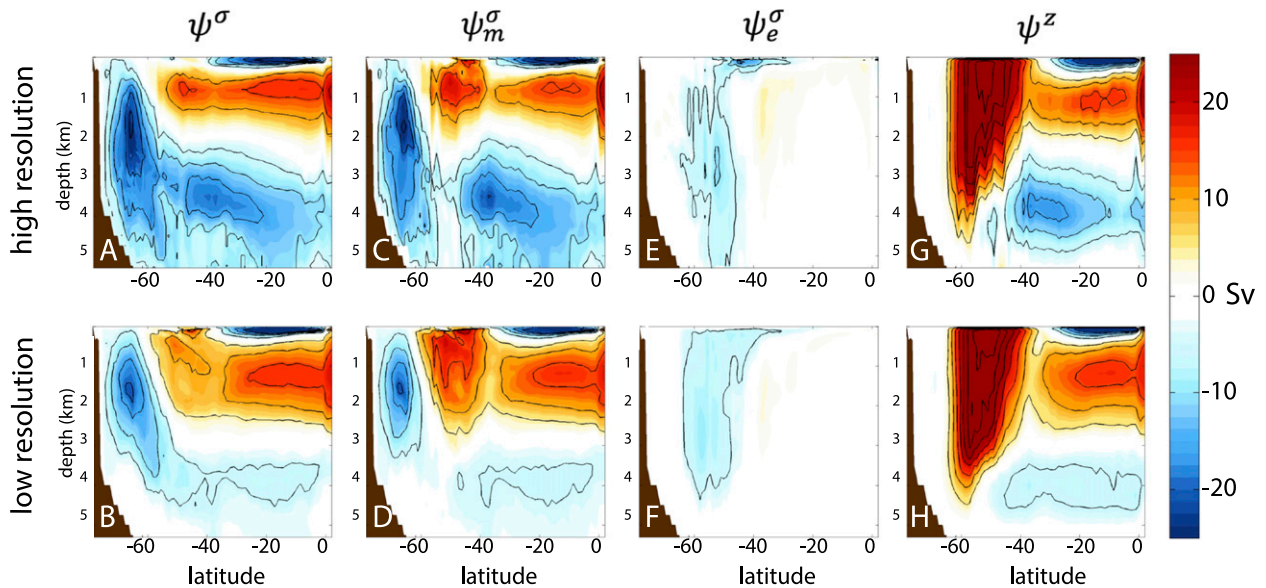
FIG. 5. Components of the MOC: (a)–(f) isopycnal overturning remapped to depth-latitude space using the zonal and time-mean isopycnal depths in the Southern Hemisphere and (g)–(h) overturning calculated in level coordinates; (top) HR and (bottom) LR. (a),(b) The total isopycnal overturning is broken into components of the (c),(d) mean isopycnal overturning and (e),(f) transient eddy-induced isopycnal overturning. Contour intervals of 5 Sv are overlaid in black.

resolution, together these processes do not result in significant resolution dependence in diapycnal volume transport, and thus large-scale circulation patterns, south of this latitude. Though some export off the Weddell continental shelf may occur northward of 64°S, Figs. 5a and 5b indicate that much of the total descent has occurred by this latitude. We conclude that the flux of dense water into the high-latitude abyssal ocean differs with resolution primarily because more of it is being made, at higher densities, at the surface in HR.

A similar breakdown of the streamfunction in the abyssal range of the lower cell can be made at 38°S (Figs. 7c,d). At either resolution, there is significant diapycnal mixing and associated adjustment of the isopycnal circulation between 64° and 38°S. The mixing between 64° and 38°S (dashed green line in Figs. 7c,d) destroys waters denser than $\sigma \sim 37.3 \, \mathrm{kg \, m^{-3}}$ in HR and $\sigma \sim 37.2 \, \mathrm{kg \, m^{-3}}$ in LR. The impact of this mixing on the circulation differs markedly between models. By 38°S, mixing redistributes volume from very dense water ($\sigma > \sim 37.15 \, \mathrm{kg \, m^{-3}}$) into the $37.15 \leq \sigma \leq 37.27 \, \mathrm{kg \, m^{-3}}$ range in HR, shifting the peak in ψ^σ toward $\sigma \sim 37.2 \, \mathrm{kg \, m^{-3}}$ but maintaining substantial northward flow. In contrast, mixing in LR lightens waters across the entire density range of the lower cell by 38°S, inducing volume fluxes toward lighter isopycnals and greatly reducing the northward flow across all density levels, evident in Fig. 5. At both resolutions, Dmix overcomes F in waters lighter

than $\sigma \sim 37.0 \, \mathrm{kg \, m^{-3}}$, reversing the direction of flow and the sign of ψ^σ.

Examination of the streamfunction components at 30°S reveals that little additional mixing occurs from 38° to 30°S at either resolution. There is a small volume flux toward lighter density classes across much of this density range at both resolutions, further reducing the magnitude of counterclockwise (negative) overturning in denser waters and increasing the magnitude of clockwise (positive) overturning for lighter waters in $\sigma_{\mathrm{lower\_cell}}$.

In sum, both surface transformation and interior transformation are key to sustaining the circulation across the latitudes sampled here, as is anticipated in a (approximate) steady state. However, the relative importance of surface and interior transformation processes, and resolution dependence therein, has a consistent spatial structure, one which may have important effects on the pattern and mechanisms of ocean heat uptake, as discussed in the next section.

To uncover the actual oceanic processes responsible for the distribution of water-mass transformation, we first consider surface transformation in more depth. Figure 6 illustrates the relative roles of heat and freshwater fluxes in transforming surface waters. Somewhat surprisingly, in light of the strong control salinity variations exert on the density of polar waters, heat loss contributes most significantly to buoyancy loss across $\sigma_{\mathrm{lower\_cell}}$ at both resolutions (but especially so in HR). Salt input contributes significantly only at very high
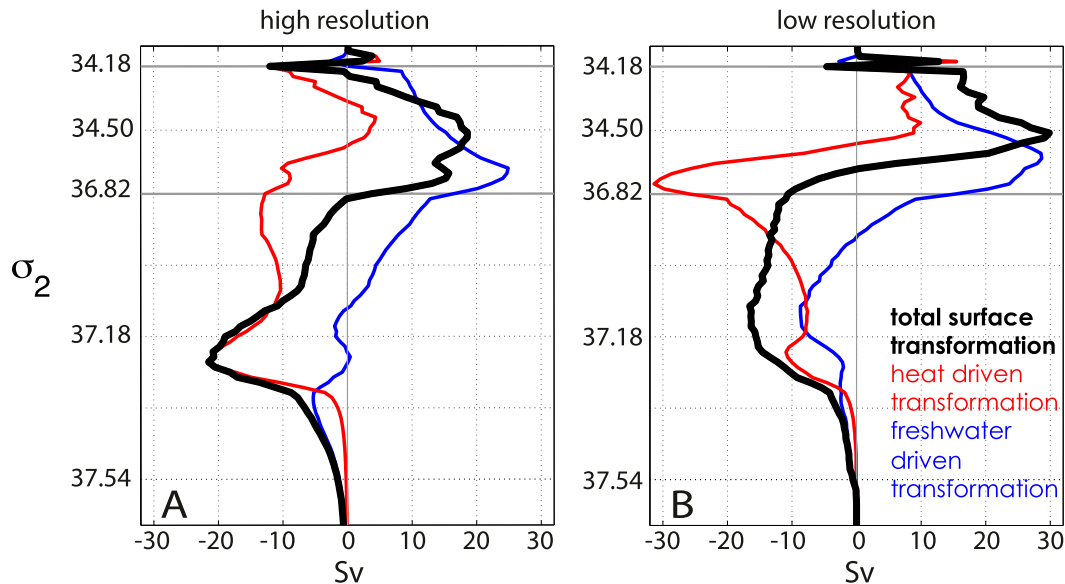
FIG. 6. Total surface water-mass transformation rate F in the Southern Ocean. The contributions from heat fluxes (red) and freshwater fluxes (blue) add up to the total (black) for (a) HR and (b) LR. The density spacing is increased for waters denser than 36.82 kg m^{-3}, which outcrop over a small area at the surface but occupy ~70% of the ocean volume south of 30°S.

densities in this density range, again particularly so in HR, though sea ice melt and precipitation are important to the transformation of lighter waters. The spatial distribution of surface transformation per unit area over several key density classes in $\sigma_{\text{lower\_cell}}$ elucidates why this is so (Fig. 8).

These "transformation maps," or distributions of diapycnal velocity, are constructed from the 20-yr mean of monthly estimates and capture the covariance of isopycnal migration and surface fluxes. These distributions demonstrate the important control isopycnal surface area has on total transformation rates [recall Eq. (4)]. Both heat and salt fluxes induce strong density gain at very high densities in the coastal polynyas of the Weddell and Ross Seas (and the entire coastal Antarctic region at decreasing densities) because of the intensity of brine rejection and the reduced control of heat fluxes on the density of very cold water. However, the total area of these coastal polynyas is relatively small, especially in HR, so the associated transformation is not substantial. The greater impact of salt rejection in LR follows from the larger spatial scale over which sea ice is formed. Perhaps counterintuitively, relatively lower surface density fluxes associated with heat loss over broader regions of the sea ice pack account for more total transformation because they act over a larger area. In LR, dense isopycnal outcrops migrate over a smaller area than in HR such that even extreme heat losses near the coast drive less total transformation at equivalent

densities. At either resolution, the Ross and Weddell Sea regions are of particular importance in part because of their southward extent: they host large areas of continental shelf and sea ice, through which dense isopycnals can maintain contact with the surface over much of the year.

Elevated rates of heat-loss-induced transformation in dense waters in HR imply larger rates of diapycnal heat convergence into these density classes. Waters in the upper 1000 m are generally colder in HR under most of the ice pack in the Ross and Weddell Seas, aside from a small region of warmer subsurface temperatures in the Ross Sea. The resolution dependency of heat transport likely results from changes in the regional circulation and diapycnal temperature gradients, though it is difficult to attribute such changes to one particular process. In both regions, the standard deviation of wintertime temperature is slightly greater in HR, which may be key to sustaining intermittent high heat loss. Variations in temperature may arise from transient features in the flow as well as fluctuations in the sea ice cover above.

Sea ice is well known to mediate rates of surface heat loss (Maykut 1982). In HR, the sea ice is thinner and less extensive than in LR, in better agreement with observations, as discussed in depth by Bryan et al. (2014). While ice thickness is likely sensitive to ocean heat transport into the ice zone, the resolution of ice dynamics also plays a central role in regulating ice thickness and thus heat loss. In HR, finely spaced grid cells
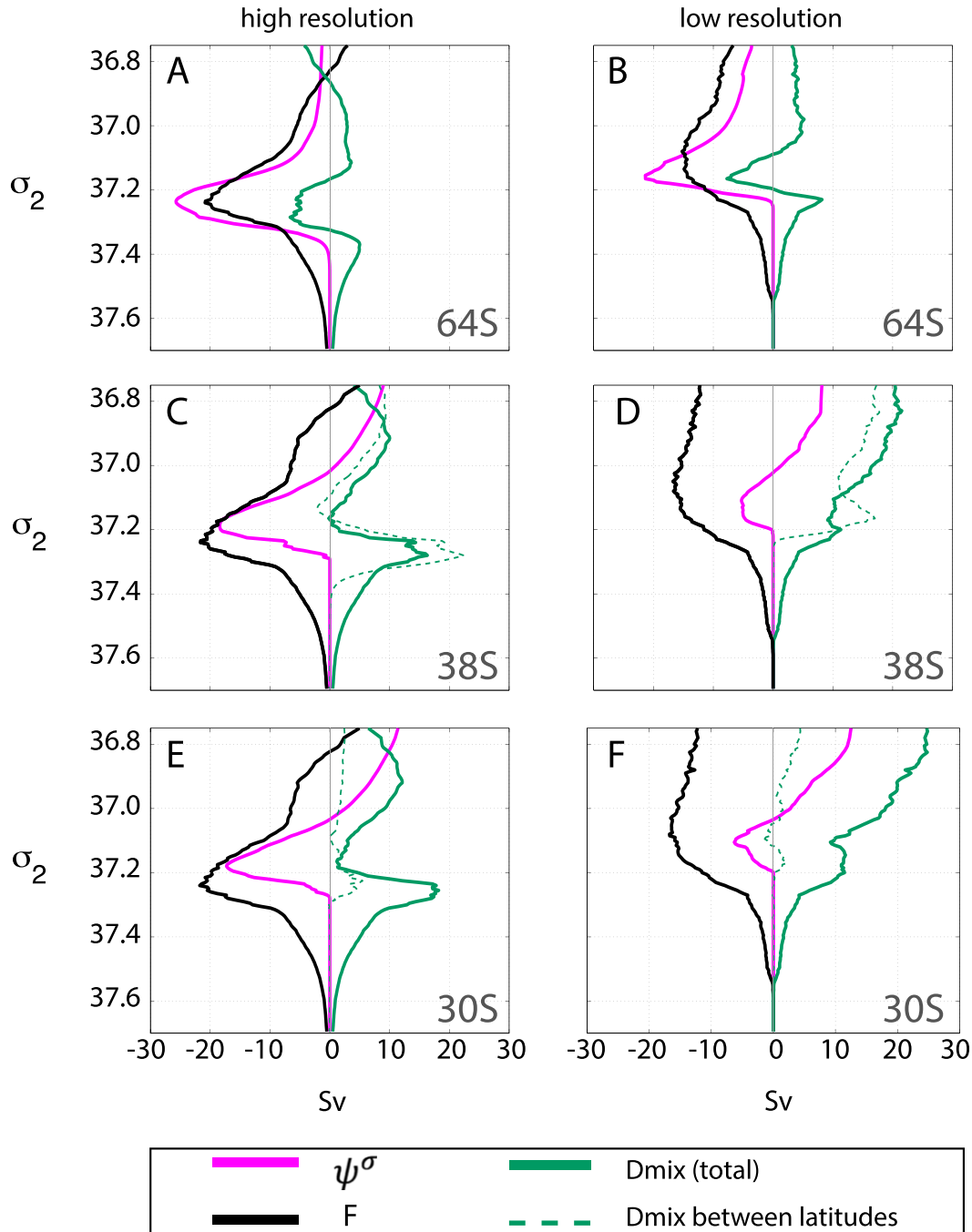
FIG. 7. Isopycnal overturning streamfunction ψ^σ (magenta) and its components from the total surface transformation F (black) and total implied mixing at each latitude Dmix (in green) at (a),(b) 65°S, (c),(d) 38°S, and (e),(f) 30°S in (left) HR and (right) LR. For convenience, the total mixing between latitude pairs (dashed green) is included (i.e., between 90° and 64°S, 64° and 38°S, and 38° and 30°S).

allow sea ice to respond to more localized atmosphere and ocean conditions, leading to more pervasive and smaller-scale coastal polynyas. This leads to higher rates of brine rejection hugging the coast, in better agreement with observations (Willmott et al. 2007). In the pack ice,

higher resolution enables a greater magnitude of divergence/convergence and shear, which creates the leads that are endemic to the observed Antarctic ice pack (Willmott et al. 2007). Lead opening exposes the ocean surface to the cold atmosphere in winter, driving

Heat-driven transformation
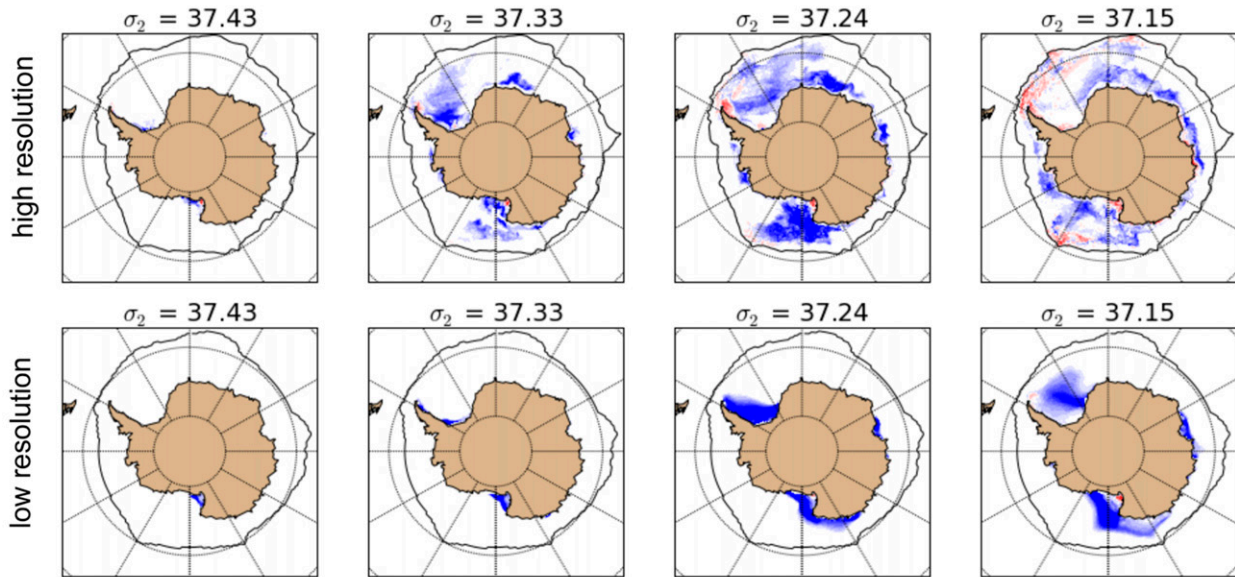
Freshwater-driven transformation
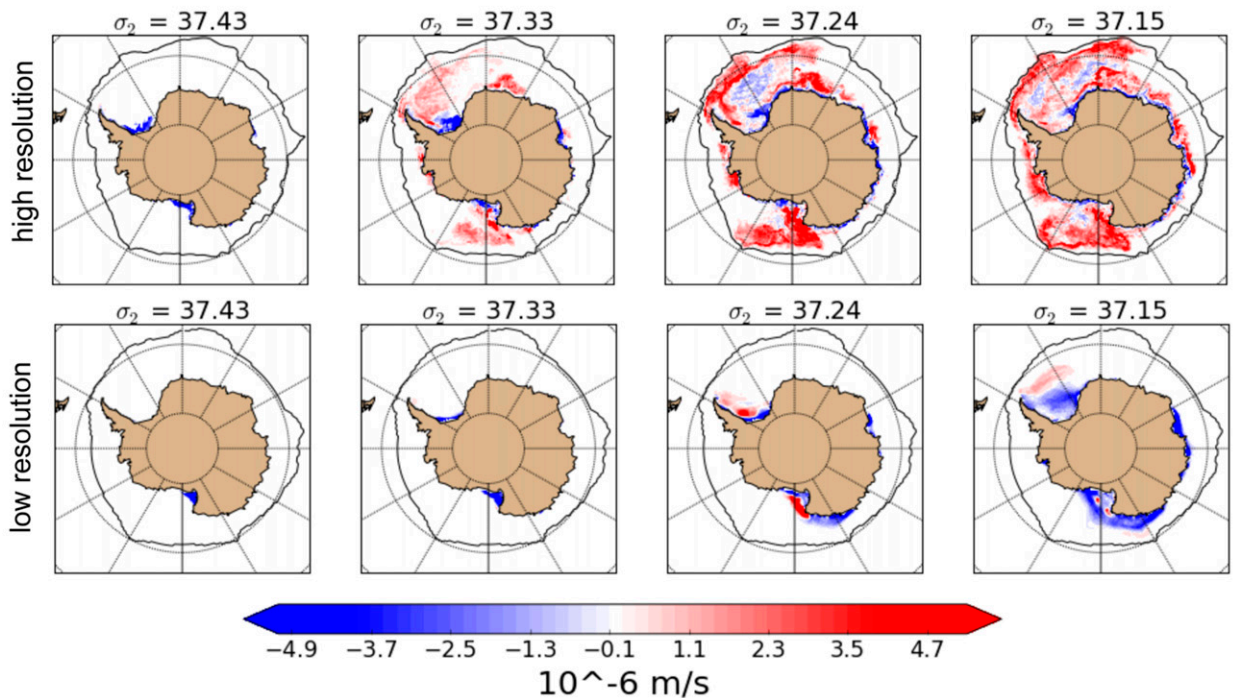
FIG. 8. Distribution of transformation per unit area (positive toward lower densities) across density surfaces (roughly spanning the density range of net volume convergence and thus surface-forced downwelling). Shown are the following: heat-driven buoyancy flux in (top) HR and (upper middle) LR and freshwater-induced buoyancy flux in (lower middle) HR and (bottom) LR.

enormous heat loss and rapid new ice formation. The resulting "frazil ice" only forms in open water (in our model) and is thus a proxy for the continuous exposure of the ocean surface. The rate of frazil ice formation has a broad peak, spanning austral fall through spring in

HR (Fig. 9a). In contrast, frazil ice formation in LR is sharply peaked in austral fall and is relatively weak in winter. The timing in LR is consistent with the northward expansion of the sea ice extent in fall, while the prolonged frazil ice production in HR indicates the
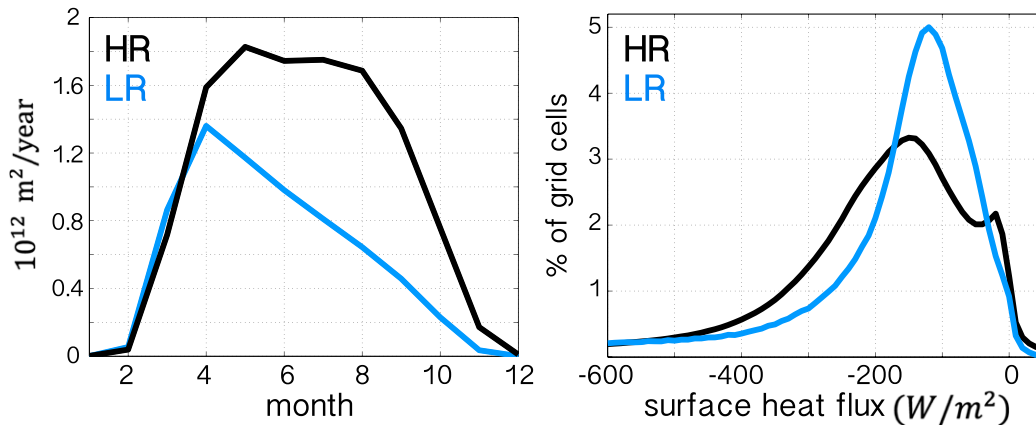
FIG. 9. (left) Monthly rates of total frazil ice formation (m^2 yr^{-1}) in HR (black) and LR (blue). (right) Distribution of area-weighted winter surface heat flux (W m^{-2}) in HR (black) and LR (blue). This distribution is calculated from monthly values during the period in which the majority of negative surface transformation occurs (June–September), within a region bounded at the north by the contour of 5% ice concentration on average for this period, though the relationship is insensitive to choice of domain. Note the skew toward more negative (out of the ocean) values in HR.

consistent opening of polynyas and leads throughout the winter. These dynamics maintain more thin ice throughout the ice-covered waters in winter in HR (not shown), which drives areas of intense heat loss, as illustrated in Figs. 8a and 9b. The extremity of heat loss experienced through the sea ice in HR contributes to the northerly transit of dense isopycnal outcrops in winter; the outcrops in LR migrate less because of the insulating effects of its thicker ice pack and less-frequent leads and polynyas.

Diagnosing the processes inducing different rates of diapycnal-mixing-driven transformation is more difficult, given our methods of calculation. Generally, models must homogenize properties like temperature and salinity over the grid scale, a consequence of discretizing a continuum; simply reducing gridcell size reduces this spurious diffusion and enables the formation of smaller-scale density gradients. This likely improves the scale of dense overflows resolved in HR, especially because bathymetry is better resolved. However, as is evident in Fig. 7, these processes have a minimal effect on altering the circulation south of 64°S, which may in part be a consequence of the small volume of the high-latitude ocean, since volume has a strong control on transformation rates.

North of 64°S, an increase in resolution significantly impacts the magnitude of mixing. The meridional flow of dense water toward the subtropics likely occurs via transient mass fluxes [e.g., see Ito and Marshall (2008); Lozier (2010)], and in deep western boundary currents (DWBC) where it is allowed by bathymetry (Orsi et al. 1999, 2002; Fukamachi et al. 2010). These boundary currents are particularly susceptible to real and numerical mixing because of their association with strong density gradients and shearing rates (Griffies et al. 2000). Mesoscale turbulence, acting to either erode or intermittently increase density gradients, likely depends on resolution, even without altering ψ_E^σ. Further, there may be different levels of numerical mixing induced across these currents; this spurious diffusion likely decreases with increasing resolution [to a degree, akin to the numerics discussed by Griffies et al. (2000)], though it persists in eddying models (Urakawa and Hasumi 2014). A representative example of the differences in DWBC characteristics between resolutions is shown at 30°S (Fig. 10), at a latitude chosen because of the large contrast in abyssal circulation strength apparent in both the isopycnal and depth-space overturning in Fig. 5. In HR, deep isopycnals slope steeply up toward the western continental boundaries or ridges, coincident with regions of strong meridional flow. The corresponding isopycnal slopes are notably flatter in LR, and the flow is much weaker. The reduced strength of these currents in LR, and associated weak abyssal overturning, follows from the elevated destruction of dense waters south of 30°S. However, Fig. 10 reveals that density gradients in HR can form on scales smaller than a single LR grid cell, indicating that correspondingly strong geostrophic currents are unresolvable in LR, even given a similar flux of dense water into the abyssal ocean. While the formation of boundary currents and the mixing that erodes them are coupled, further unraveling their interactions is beyond the scope of this article.
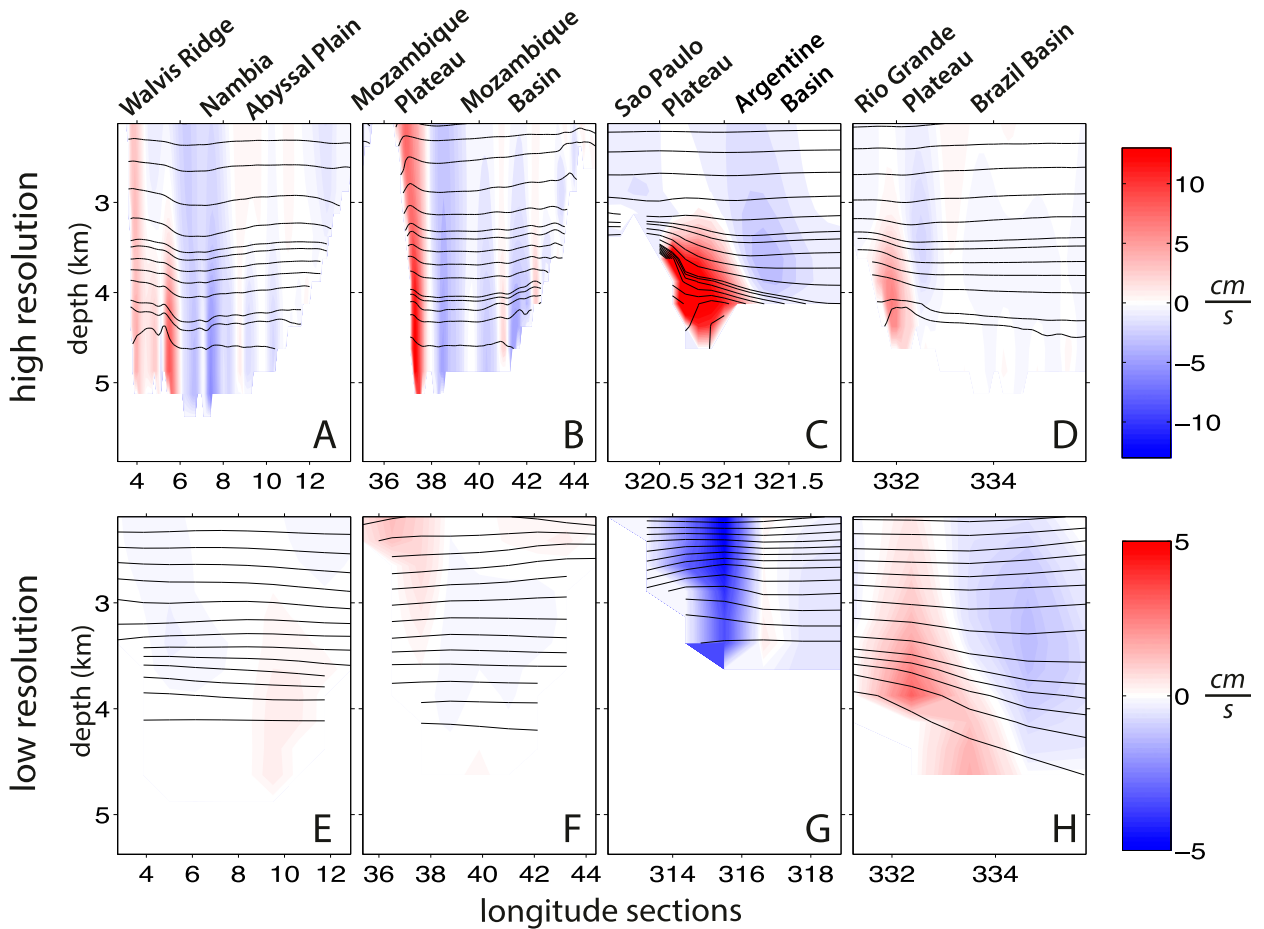
FIG. 10. Zonal transects across key deep western boundary currents at 30°S as a function of longitude and depth (below 3000 m). The meridional velocity (color) is overlaid with isopycnals (black) in (a)–(d) HR and (e)–(f) LR. Positive (red) is northward. Isopycnal spacing varies with stratification, but is on average 0.01 kg m^{-3}. Bathymetric features are noted to orient the reader. Note the reduced color scale for LR.

As a final diagnostic of the Southern Ocean circulation state and its dependence on resolution, we consider the 20-yr average integrated heat content tendency for a control volume bounded at 30°S, below each depth z^*, and spanning all longitudes. For HR,

$$-\frac{c_p \rho_o}{(t_1 - t_0)} \int_{t_0}^{t_1} \int_{90°S}^{30°S} \int_x \int_{-B(x,y)}^{z^*} \left\{ \left(\frac{\partial\theta}{dt}\right)_1 + \left[\nabla\cdot(\overline{u}\,\overline{\theta}) + \frac{\partial}{\partial z}\overline{(w\theta)}\right]_2 \right. $$
$$\left. + \left(\nabla\cdot\overline{u'\theta'} + \frac{\partial}{\partial z}\overline{w'\theta'}\right)_3 - \left[\frac{\partial}{\partial z}\left(\kappa_{\text{bg}}\frac{\partial\overline{\theta}}{\partial z}\right)\right]_4 - \left[\frac{\partial}{\partial z}\left(\kappa_{\text{ML}}\frac{\partial\overline{\theta}}{\partial z}\right)\right]_5 \right\} dx\,dy\,dz\,dt = 0; \tag{7}$$

and for LR,

$$-\frac{c_p \rho_o}{(t_1 - t_0)} \int_{t_0}^{t_1} \int_{90°S}^{30°S} \int_x \int_{-B(x,y)}^{z^*} \left\{ \left(\frac{\partial\theta}{dt}\right)_1 + \left[\nabla\cdot\overline{(u\theta)} + \frac{\partial}{\partial z}\overline{(w\theta)}\right]_2 \right. $$
$$\left. + \left(\nabla\cdot\overline{u_b\theta} + \frac{\partial}{\partial z}\overline{w_b\theta}\right)_3 - \left[\frac{\partial}{\partial z}\left(\kappa_{\text{bg}}\frac{\partial\overline{\theta}}{\partial z}\right)\right]_4 - \left[\frac{\partial}{\partial z}\left(\kappa_{\text{ML}}\frac{\partial\overline{\theta}}{\partial z}\right) - \nabla\cdot\mathbf{K}_{\text{redi}}\nabla\theta\right]_5 \right\} dx\,dy\,dz\,dt = 0. \tag{8}$$
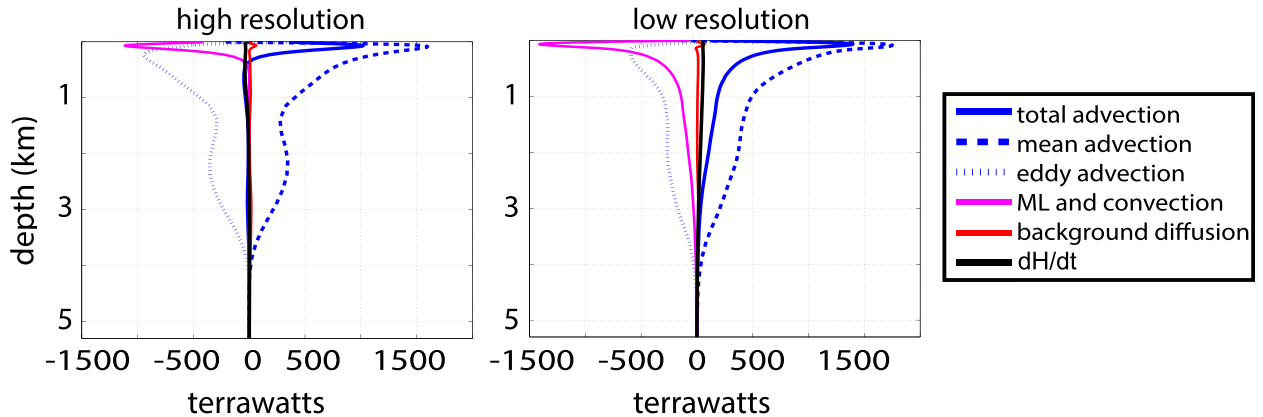
FIG. 11. Relative contributions to the heat content tendency of the ocean volume below depth z^*, south of 30°S in (left) HR and (right) LR. As defined in the legend at right, the total heat content will depend on total advective fluxes (solid blue); mean advective fluxes (dashed blue); eddy advective fluxes (short dashed blue); diffusive fluxes (red); mixed-layer, convective, and (in LR) Redi fluxes (magenta) and result in a very small temperature tendency (black solid). Fluxes are defined as positive downward.

Note that the sign convention is such that positive vertical fluxes across the upper bounding surface z^* act to increase the heat content of the control volume. Here $\theta = \theta(x, y, z, t)$ is potential temperature; $u = u(x, y, z, t)$ and $w = w(x, y, z, t)$ are the horizontal and vertical velocity, respectively; an overbar denotes a time mean; the prime denotes a deviation from the time mean; the subscript b denotes a bolus field in LR; c_p is the specific heat capacity for seawater; and ρ_o is a reference density. Plotted in Fig. 11 is the heat content tendency (labeled $\partial H/\partial t$) associated with the temperature trend (term 1). This tendency will depend on the following: heat transport by the mean flow (term 2); the transient eddy-induced flow (term 3); the background vertical diffusion, dependent on the background diffusivity, κ_{bg} (term 4); and a residual term that captures the remaining mixing processes, like KPP mixed-layer (ML) processes and convection (term 5). In LR, this residual term also includes the parameterized along-isopycnal diffusion (the Redi flux, dependent on the parameterized isopycnal diffusivity tensor $\mathbf{K}_{redi}$). Thus, part of the impact of mesoscale eddies on the vertical heat budget is captured in this residual term in LR; the Redi fluxes could not be directly calculated because the time-dependent diffusivity tensor was not saved in the monthly output files. While there is a small trend in heat content at either resolution, in the top 500 m, advective warming nearly balances convective cooling. Below this depth, to first order at either resolution, eddy heat fluxes are sufficient to counter heat fluxes by the mean flow, emphasizing the importance of eddies in diffusing heat across strong temperature gradients. This breakdown of heat fluxes will be useful in the subsequent section to elucidate the physics responsible for deep ocean warming under greenhouse forcing.

4. Carbon dioxide doubling response

We now show how resolution affects the response of the Southern Ocean in the 20 yr of carbon dioxide stabilization after doubling. The Southern Hemisphere surface air temperatures increase at both resolutions: air temperatures in the high southern latitudes warm by up to 8°C over some regions of the ocean and sea ice pack. Bryan et al. (2014) discuss how climate change depends on resolution more generally; here, we focus on the deep Southern Ocean's response.

At both resolutions, the lower cell of the isopycnal MOC slows substantially in response to surface warming (Fig. 12), though this reduction is notably greater in HR. The response of the overturning $\Delta\psi^\sigma$ is dominated by a reduction in the circulation strength in the subpolar range of the lower cell, with smaller changes across the abyssal range. The resolution dependence of the response to carbon dioxide doubling is primarily a feature of the mean isopycnal flow $\Delta\psi^\sigma_M$; while the transient eddy-induced circulation response to carbon dioxide doubling $\Delta\psi^\sigma_E$ depends somewhat on resolution, it is comparatively small.

Surface warming and the associated changes in freshwater fluxes alter the surface water-mass transformation ΔF (see Fig. 13). There is a significant (positive) anomaly in ΔF across the outcrops of the lower cell. To understand the impact of these surface changes relative to changes in interior transformation, we compare changes in the strength of processes contributing to the circulation response throughout the density range of the
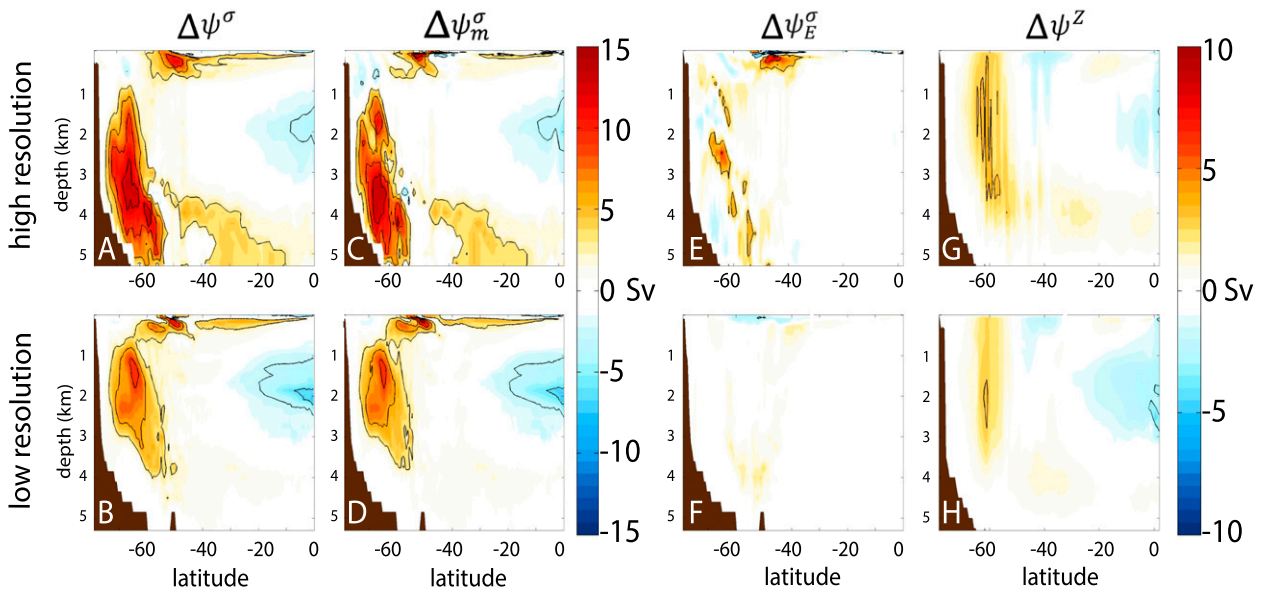
FIG. 12. As in Fig. 5, but the anomaly in response to doubling carbon dioxide (i.e., perturbed − control). Contour intervals of 3 Sv are overlaid in black. Note reduced color scale for (e)–(h) the eddy-induced and depth-space circulation changes.

lower cell. Because the carbon dioxide forcing was only stabilized for 20 yr, the response is transient, and the isopycnal volume inflation is nonnegligible. Thus, the response to carbon dioxide doubling apparent in the overturning $\Delta\psi^\sigma$ includes the contributions from changes in isopycnal volume $\Delta\partial V/\partial t$, surface water-mass transformation ΔF, and implied interior mixing $\Delta D\text{mix}$ (see Fig. 14). In both LR and HR, the significant $\Delta\psi^\sigma$ at 64°S can be primarily attributed to ΔF; this affirms the

close connection between surface transformation and flow in the subpolar range as diagnosed in the control climate. Further, $\Delta D\text{mix}$ at 64°S is largely explained by the magnitude and pattern of ΔF. In other words, the reduction in shelf water mixing directly reflects the reduction in shelf water production. Farther to the north, at 38°S, there is little $\Delta\psi^\sigma$ at either resolution. The large change in mixing-driven transformation between these latitudes (which is primarily a reduction in the
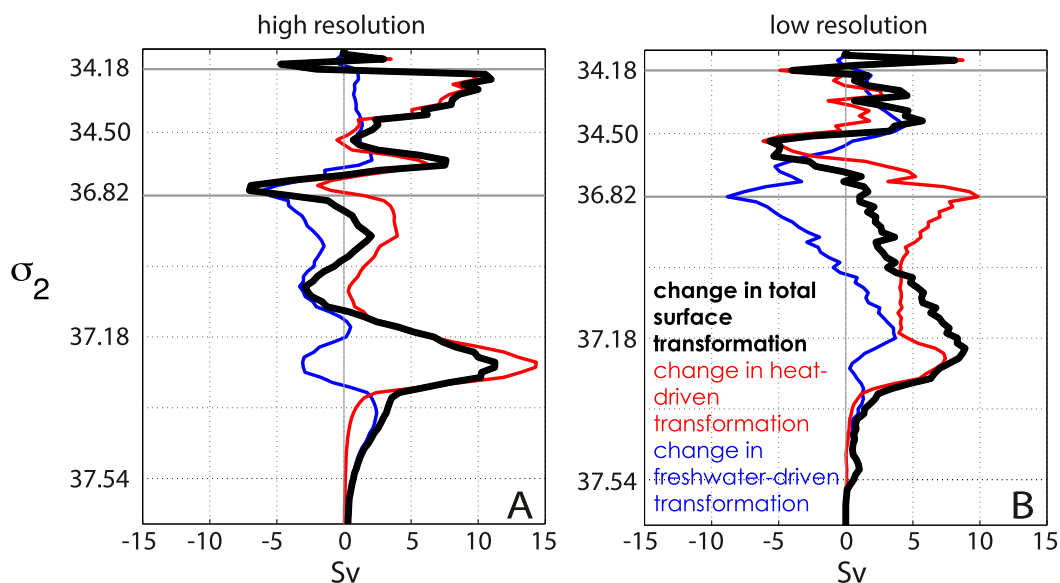

FIG. 13. As in Fig. 6, but the anomaly in response to doubling carbon dioxide (i.e., perturbed − control).
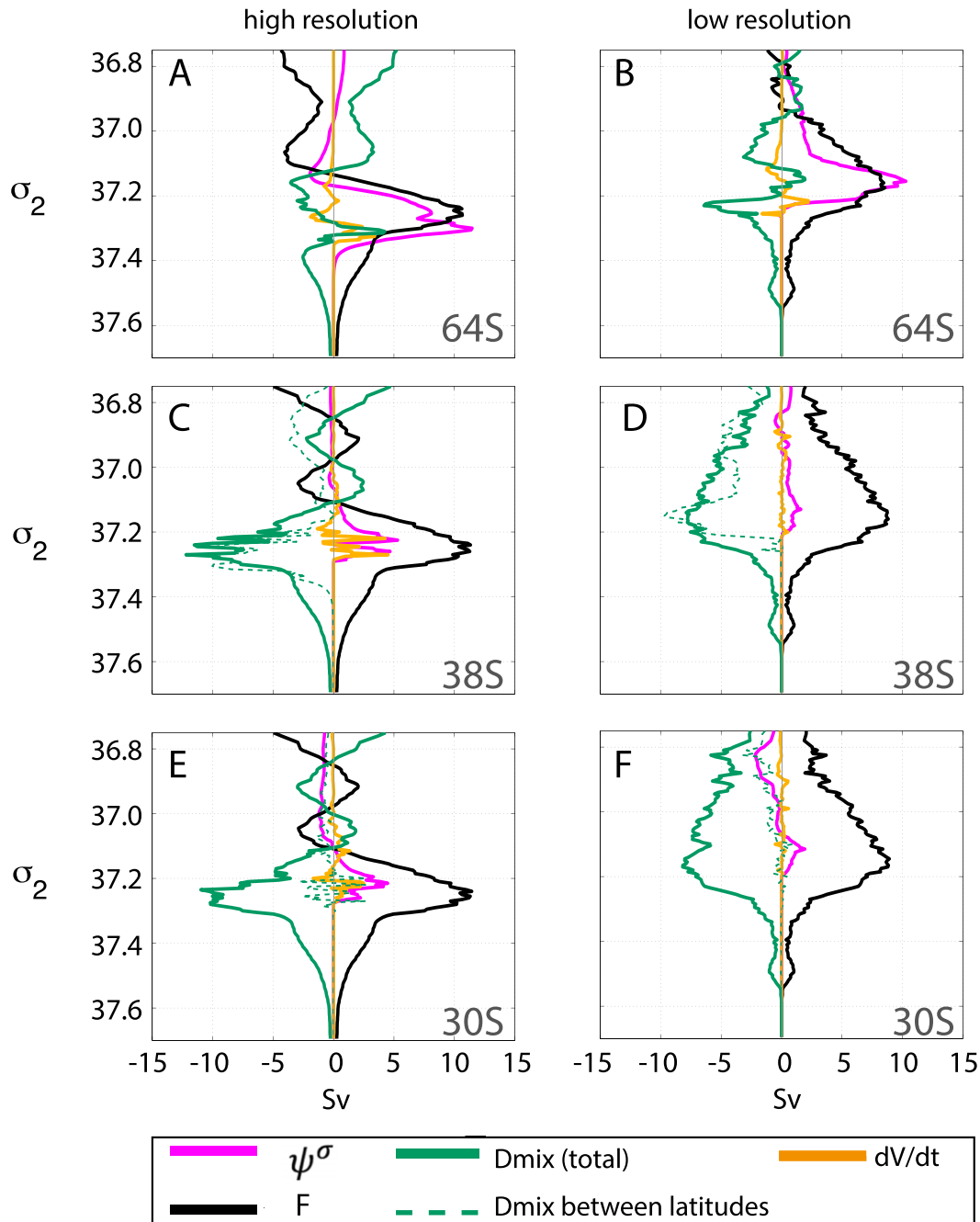
FIG. 14. As in Fig. 7, but the anomaly in response to doubling carbon dioxide (i.e., perturbed − control). In addition, the anomalous response of the isopycnal volume inflation is shown in gold.

effectiveness of mixing in the control simulations, i.e., of the same shape but of opposite sign) can again be explained as the result of a reduction in downwelling dense waters. Farther north yet, at 30°S, $\Delta\psi^\sigma$ is increasingly small, implying a very small reduction in mixing between 38° and 30°S. Greater changes at these latitudes may occur over time, as the influence of high-latitude

processes spreads northward; however, such changes are not captured in our simulations. There is some redistribution of isopycnal volume from very dense to slightly less dense water classes, though it is small compared with ΔF.

In the control, $\Delta\psi^\sigma$ is sustained by both F and Dmix, though the influence of each varies with latitude. In
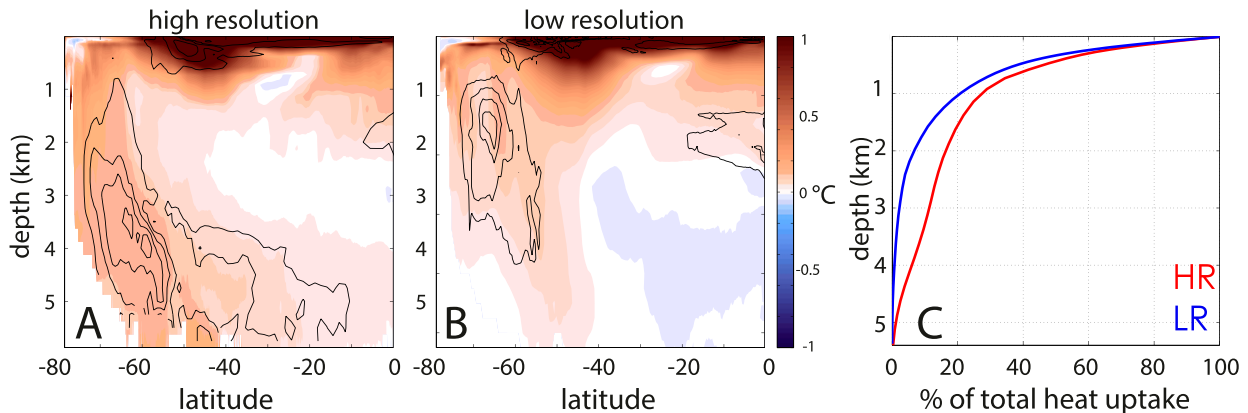
FIG. 15. (a)–(b) Zonally averaged temperature change for the Southern Hemisphere in (a) HR and (b) LR, overlaid with contours of the anomalous isopycnal MOC streamfunction at 3, 6, 9, and 12 Sv; and (c) cumulative fraction of heat uptake south of the equator in HR (red) and LR (blue).

contrast, these transient results suggest that the $\Delta\psi^\sigma$ is almost entirely explained by a reduction in surface transformation, particularly so in the subpolar range. Further, the resolution dependence of ΔF primarily explains the resolution dependence of $\Delta\psi^\sigma$. Since the pattern of ΔF is both more peaked and confined to denser isopycnals in HR, $\Delta\psi^\sigma$ in HR is larger and extends deeper in the water column than in LR. In HR, this peak is ~15 Sv and is centered at an average depth of 3.8 km; in LR, the peak reduction is ~12 Sv and is centered at an average depth of 1.7 km.

The surface transformation function response to carbon dioxide doubling is largely attributed to a reduction in surface heat fluxes. We interpret this as follows: in a warmer climate, there is a reduction in the air–sea temperature contrast in the coastal ocean, especially in wintertime, inducing a reduction in heat lost through the sea ice pack. The reduction in heat loss in response to carbon dioxide doubling is strongest in the winter months, and the (positive) anomaly in surface transformation occurs almost entirely in winter. Surface warming also drives a thinning of the ice pack irrespective of resolution. Sea ice volume is reduced by 40% in LR and 26% in HR. While there is some decrease in ice extent at each resolution, this volume reduction is mainly caused by changes in ice thickness. This relatively greater thinning in LR is characteristic of thicker ice in the mean state (Bitz and Roe 2004). Because thinner ice is less insulating, thinning provides a damping effect on what would otherwise be a larger reduction in heat loss in response to warming air temperatures. This damping effect is greater in LR because of the more substantial thinning in LR, revealing how sensitive the response to carbon dioxide doubling of the sea ice–atmosphere–ocean system can be to the mean state ice

thickness. Last, larger changes in the meridional circulation in HR may reduce the rate of heat convergence into very dense waters in this region. The shape of the anomaly in surface transformation is also impacted by a shift in the spatial distribution in surface densities. These combined changes drive the larger reduction in surface water-mass transformation across a narrower range of denser waters in HR (note the differences in positive anomalies peaked around $37.25\,kg\,m^{-3}$ in HR and $37.18\,kg\,m^{-3}$ in LR). A shift in the density classes into which sea ice melts partially offsets the strong reduction in buoyancy loss from reduced heat loss in slightly lighter waters.

The circulation response to carbon dioxide doubling, and the sensitivity of each model to surface transformation changes, leads to a strikingly different distribution of ocean warming with resolution, particularly in the high-latitude abyssal ocean. Figures 15a and 15b illustrate the zonal-average temperature change with depth. In HR, warming extends along the path of dense water formation, from the coast into the abyssal ocean. In LR, warming is confined to the surface and mid-depths, with nearly no warming of the abyssal ocean below 3500 m. These warming patterns lead to important differences in the total heat uptake with depth in the Southern Ocean (Fig. 15c). Changes in heat content are primarily explained by anomalous advective heat fluxes, as illustrated in Fig. 16. In HR, the total advective warming into the ocean volume south of 30°S is a result of anomalous positive vertical and horizontal eddy heat fluxes and anomalous vertical fluxes by the mean flow, which are partially compensated by anomalous negative horizontal fluxes by the mean flow (not shown). In LR, the total advective warming is primarily a result of anomalous vertical eddy fluxes, which are also partially compensated by anomalous negative horizontal fluxes
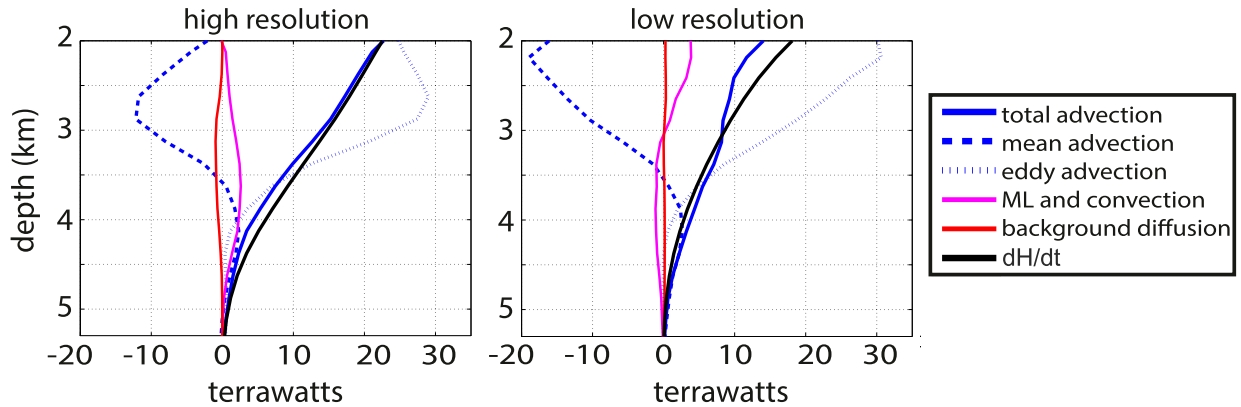
FIG. 16. As in Fig. 11, but the anomaly in response to doubling carbon dioxide (i.e., perturbed − control).

by the mean flow. As can be seen in Fig. 15, the pattern of warming bears a close connection with circulation changes, which are in turn intrinsically related to the control state circulation. The relative magnitude of the control MOC strength (ψ^{σ}) versus the magnitude of its reduction ($\Delta\psi^{\sigma}$) is important in explaining why heat uptake differs across models (Banks and Gregory 2006; Xie and Vallis 2012; Rugenstein et al. 2013; Kostov et al. 2014). We attempt to address this by partitioning the total heat flux response to carbon dioxide doubling as

$$\Delta(vT) = T\Delta v + v\Delta T + \text{HOT}, \qquad (9)$$

where HOT stands for higher-order terms. Because we cannot calculate submonthly correlations between velocity and temperature, our calculations of the relative roles of eddy heat flux response are imperfect. With this caveat, we find that the total advective heat flux response due to changes in MOC strength, via Δv, is responsible for 2–3 times (depending on the depth) more of the warming below 2000 m than changes in the temperature field ΔT. Thus, a redistribution of ocean heat by the circulation response to doubling carbon dioxide is a key component of Southern Ocean warming.

5. Discussion and conclusions

These results support the notion that model resolution fundamentally alters simulated Southern Ocean dynamics. This possibility has been explored in numerous studies (e.g., Henning and Vallis 2005; Hallberg and Gnanadesikan 2006; Farneti et al. 2010; Abernathey et al. 2011; Bryan et al. 2014; Farneti et al. 2014), which have justifiably focused on the first-order effects of transient eddies on the residual circulation. In our experiments, the transient eddy-induced meridional circulation varies little with resolution, reinforcing findings

by Gent and Danabasoglu (2011) and Gent (2016), who argued that employing an unconstrained spatially varying GM coefficient greatly improves the agreement between the resolved and parameterized contribution of transient eddies to the circulation.

Here, we call attention to the influence of increased model resolution on the behavior of other fundamental small-scale processes, in particular sea ice divergence and shear and the formation of small-scale ocean density gradients and flows. These processes are generally only resolved to the extent that grid spacing permits, without additional subgrid-scale parameterizations. The increased resolution of these processes has a major influence on the mean isopycnal flow of the lower cell in this model. To quantify the spatial distribution of processes sustaining this circulation, and contributing to circulation differences with resolution, we consider the evolution of water-mass transformation (see, e.g., Walin 1982) across latitudes of the Southern Ocean and focus on lower cell density classes. We conclude that downwelling near Antarctica is consistent with heat loss from isopycnal outcrops in the vicinity of leads in the sea ice pack, the simulation of which is greatly improved by increased resolution: these finescale, intermittent sea ice openings (polynyas and leads) are more frequent at higher resolution, enabling vast areas of thinner ice and more efficient surface heat loss over localized scales. Greater heat loss from very dense isopycnals at high resolution is sustained by a greater diapycnal convergence of heat into these density classes by the flow. The resolution dependence of transient eddy fluctuations across the shelf front (i.e., Stewart and Thompson 2013) may play a role in diapycnal heat fluxes. However, even our higher-resolution experiment is too coarse to explicitly resolve their dominant scales at the shelf front.

As water flows northward from the shelf regions into the abyssal ocean, transformation from diapycnal

mixing processes contributes increasingly to patterns of flow. Progressively greater interior transformation is expected as the volume of most density classes increases over the immediate domain northward from the continental shelves; correspondingly distinct patterns of interior transformation between resolutions emerge as different dynamics act on progressively larger volumes of water. Our higher-resolution case forms more vigorous, small-scale DWBCs and experiences less diapycnal mixing of dense waters, sustaining a stronger abyssal circulation; vigorous mixing damps abyssal overturning strength dramatically at lower resolution. These differences may be tied in part to a reduction in numerical mixing, though such mixing can persist in eddying models (Urakawa and Hasumi 2014).

In the approximate steady state of our control simulation, processes regulating the transformation of seawater at the surface and in the interior together sustain the lower cell circulation. In contrast, we attribute changes in flow in response to a doubling of carbon dioxide predominantly to reductions in surface transformation. While the reduction in surface transformation leads to a dramatic reduction in overturning irrespective of resolution (14 Sv at high resolution, a reduction of ~54%, and ~10 Sv at lower resolution, a reduction of ~45%), these overturning changes are greater and deeper on average at high resolution because of a larger reduction in heat-loss-induced transformation. There is a decrease in diapycnal mixing throughout the abyssal Southern Ocean with carbon dioxide doubling, though the magnitude of this decrease directly reflects reduction in upstream dense water production at the surface. These results emphasize an important aspect in the dynamics of the lower cell circulation omitted from several theoretical and idealized studies (e.g., Ito and Marshall 2008; Nikurashin and Vallis 2011, 2012). While these studies include a simplified form of buoyancy loss in the high latitudes, they do not include a theory for the sensitivity of the circulation to changes in surface fluxes. In the absence of any evolving surface buoyancy forcing, their results stress the lower cell's sensitivity to other processes: particularly, changes in southward eddy heat fluxes across the ACC, westerly wind strength, and abyssal mixing rates. These insights are crucial to understanding the system but have limitations. Our results suggest that the lower cell circulation is most sensitive, at least in a "global warming" type of perturbation, to changes in surface heat loss with atmospheric warming and that this heat loss is sensitive to surface processes. This is supported in the conceptual frameworks of Shakespeare and Hogg (2012) and Stewart et al. (2014) and in the eddy-permitting model discussed by Kuhlbrodt et al. (2015). Further, the relationship between southward

eddy heat fluxes and MOC strength becomes more convoluted in a framework that includes evolving interactions with the atmosphere. In fact, southward eddy heat fluxes across the ACC are lower in our high-resolution control experiment (Bryan et al. 2014), while the lower cell is stronger. It is possible that the influence of abyssal mixing rates, as mediated by southward eddy heat fluxes, and westerly winds strength, are overemphasized, or misrepresented, in models that do not include realistically responsive surface fluxes.

The omission of evolving surface fluxes may alter mechanisms of heat uptake. Zhang and Vallis (2013) consider the impact of model resolution on ocean heat uptake in an idealized ocean-only model, which imposed surface heat fluxes and included neither sea ice nor the dependence of density on salinity. They attribute the greater abyssal heat uptake simulated in their higher-resolution model to the greater advection of heat by the stronger mean state circulation, explained as a result of higher eddy heat fluxes across the ACC. In contrast, we find that circulation changes significantly redistribute the existing internal heat reservoir in our model in response to surface changes. This redistribution of heat is a larger component of abyssal Southern Ocean warming than the advection of anomalous heat taken up at the surface in these simulations, in agreement with the results of Xie and Vallis (2012).

Our results also suggest a possible shortcoming in the behavior of many standard-resolution coupled models. Marshall et al. (2015) studied Southern Ocean heat uptake across a range of standard-resolution CMIP5 models and found that the dominant mechanism for Southern Ocean heat uptake in these models was the northward advection, and ultimate subduction, of anomalous heat taken up at the Southern Ocean surface and resulting in warming in the upper 1500–2000 m (Marshall et al. 2014). This mechanism of heat uptake is certainly active in our model, as evident by the significant mode water warming around 65°–35°S (Figs. 15a,b). However, while the heat uptake of the Southern Ocean varies little with resolution (2.5×10^{23} J at high resolution and 2.4×10^{23} J at low resolution), more of this heat enters the lower cell in our high-resolution experiment. This changes the distribution of heat with depth (Fig. 15c) as well as the circulation regime in which this anomalous heat resides. The models analyzed by Marshall et al. (2015) produce unrealistically small volumes of, or spuriously formed, AABW (Heuzé et al. 2013). Our results raise the possibility that the response of standard-resolution models to surface warming may be biased because of their inability to (realistically) simulate abyssal ocean warming, and instead these models warm too vigorously in the mode waters

closer to the ocean surface. In other words, models with weaker lower cells versus those with stronger lower cells may have intrinsically different capacities to suppress surface warming over long time scales, as has been suggested for the AMOC (Winton et al. 2014). While temperature is not a passive tracer, the time scales at which anomalously warm interior waters might be expected to eventually alter SSTs likely differ for abyssal and mode waters because of their different residence times (i.e., Gebbie and Huybers 2012). Since radiative feedbacks are influenced by SST (Winton et al. 2010), a bias in the fate of heat taken up at the Southern Ocean surface could alter the evolution of transient climate change (Armour et al. 2013). We leave exploration of this possibility to future studies.

REFERENCES

Abernathey, R., and C. Wortham, 2015: Phase speed cross spectra of eddy heat fluxes in the eastern Pacific. *J. Phys. Oceanogr.*, **45**, 1285–1301, doi:10.1175/JPO-D-14-0160.1.

——, J. Marshall, and D. Ferreira, 2011: The dependence of Southern Ocean meridional overturning on wind stress. *J. Phys. Oceanogr.*, **41**, 2261–2278, doi:10.1175/JPO-D-11-023.1.

Abraham, J. P., C. M. Domingues, J. T. Fasullo, J. Gilson, G. Goni, S. A. Good, and J. M. Gorman, 2013: A review of global ocean temperature observations: Implications for ocean heat content estimates and climate change. *Rev. Geophys.*, **51**, 450–483, doi:10.1002/rog.20022.

Armour, K. C., C. M. Bitz, and G. H. Roe, 2013: Time-varying climate sensitivity from regional feedbacks. *J. Climate*, **26**, 4518–4534, doi:10.1175/JCLI-D-12-00544.1.

Ballarotta, M., S. Drijfhout, T. Kuhlbrodt, and K. Döös, 2013: The residual circulation of the Southern Ocean: Which spatio-temporal scales are needed? *Ocean Modell.*, **64**, 46–55, doi:10.1016/j.ocemod.2013.01.005.

Banks, H. T., and J. M. Gregory, 2006: Mechanisms of ocean heat uptake in a coupled climate model and the implications for tracer based predictions of ocean heat uptake. *Geophys. Res. Lett.*, **33**, L07608, doi:10.1029/2005GL025352.

Bitz, C. M., and G. H. Roe, 2004: A mechanism for the high rate of sea ice thinning in the Arctic Ocean. *J. Climate*, **17**, 3623–3632, doi:10.1175/1520-0442(2004)017<3623:AMFTHR>2.0.CO;2.

——, and L. M. Polvani, 2012: Antarctic climate response to stratospheric ozone depletion in a fine resolution ocean climate model. *Geophys. Res. Lett.*, **39**, L20705, doi:10.1029/2012GL053393.

Bryan, F. O., 1987: Parameter sensitivity of primitive equation ocean general circulation models. *J. Phys. Oceanogr.*, **17**, 970–985, doi:10.1175/1520-0485(1987)017<0970:PSOPEO>2.0.CO;2.

——, G. Danabasoglu, N. Nakashiki, Y. Yoshida, D.-H. Kim, J. Tsutsui, and S. C. Doney, 2006: Response of the North Atlantic thermohaline circulation and ventilation to increasing carbon dioxide in CCSM3. *J. Climate*, **19**, 2382–2397, doi:10.1175/JCLI3757.1.

——, P. R. Gent, and R. Tomas, 2014: Can Southern Ocean eddy effects be parameterized in climate models? *J. Climate*, **27**, 411–425, doi:10.1175/JCLI-D-12-00759.1.

Cummins, P. F., G. Holloway, and E. Gargett, 1990: Sensitivity of the GFDL Ocean General Circulation Model to a parameterization of vertical diffusion. *J. Phys. Oceanogr.*, **20**, 817–830, doi:10.1175/1520-0485(1990)020<0817:SOTGOG>2.0.CO;2.

Danabasoglu, G., and J. C. McWilliams, 1995: Sensitivity of the global ocean circulation to parameterizations of mesoscale tracer transports. *J. Climate*, **8**, 2967–2987, doi:10.1175/1520-0442(1995)008<2967:SOTGOC>2.0.CO;2.

——, and J. Marshall, 2007: Effects of vertical variations of thickness diffusivity in an ocean general circulation model. *Ocean Modell.*, **18**, 122–141, doi:10.1016/j.ocemod.2007.03.006.

——, S. C. Bates, B. P. Briegleb, S. R. Jayne, M. Jochum, W. G. Large, S. Peacock, and S. G. Yeager, 2012: The CCSM4 ocean component. *J. Climate*, **25**, 1361–1389, doi:10.1175/JCLI-D-11-00091.1.

de Lavergne, C., G. Madec, J. Le Sommer, A. J. G. Nurser, and A. C. Naveira Garabato, 2016: The impact of a variable mixing efficiency on the abyssal overturning. *J. Phys. Oceanogr.*, **46**, 663–681, doi:10.1175/JPO-D-14-0259.1.

Döös, K., and D. Webb, 1994: The Deacon cell and other meridional cells of the Southern Ocean. *J. Phys. Oceanogr.*, **24**, 429–442, doi:10.1175/1520-0485(1994)024<0429:TDCATO>2.0.CO;2.

Dufour, C. O., L. L. Sommer, J. D. Zika, M. Gehlen, J. C. Orr, P. Mathiot, and B. Barnier, 2012: Standing and transient eddies in the response of the Southern Ocean meridional overturning to the southern annular mode. *J. Climate*, **25**, 6958–6974, doi:10.1175/JCLI-D-11-00309.1.

Farneti, R., T. L. Delworth, A. J. Rosati, S. M. Griffies, and F. Zeng, 2010: The role of mesoscale eddies in the rectification of the Southern Ocean response to climate change. *J. Phys. Oceanogr.*, **40**, 1539–1557, doi:10.1175/2010JPO4353.1.

——, S. Dwivedi, F. Kucharski, F. Molteni, and S. M. Griffies, 2014: On Pacific subtropical cell variability over the second half of the twentieth century. *J. Climate*, **27**, 7102–7112, doi:10.1175/JCLI-D-13-00707.1.

——, and Coauthors, 2015: An assessment of Antarctic Circumpolar Current and Southern Ocean meridional overturning circulation during 1958–2007 in a suite of interannual CORE-II simulations. *Ocean Modell.*, **93**, 84–120, doi:10.1016/j.ocemod.2015.07.009.

Fukamachi, Y., S. R. Rintoul, J. A. Church, S. Aoki, S. Sokolov, M. A. Rosenberg, and M. Wakatsuchi, 2010: Strong export of Antarctic Bottom Water east of the Kerguelen Plateau. *Nat. Geosci.*, **3**, 327–331, doi:10.1038/ngeo842.

Gebbie, G., and P. Huybers, 2012: The mean age of ocean waters inferred from radiocarbon observations: Sensitivity to surface

sources and accounting for mixing histories. *J. Phys. Oceanogr.*, **42**, 291–305, doi:10.1175/JPO-D-11-043.1.

Gent, P. R., 2016: Effects of Southern Hemisphere wind changes on the meridional overturning circulation in ocean models. *Annu. Rev. Mar. Sci.*, **8**, 79–94, doi:10.1146/annurev-marine-122414-033929.

——, and J. C. McWilliams, 1990: Isopycnal mixing in ocean circulation models. *J. Phys. Oceanogr.*, **20**, 150–155, doi:10.1175/1520-0485(1990)020<0150:IMIOCM>2.0.CO;2.

——, and G. Danabasoglu, 2011: Response to increasing Southern Hemisphere winds in CCSM4. *J. Climate*, **24**, 4992–4998, doi:10.1175/JCLI-D-10-05011.1.

——, S. G. Yeager, R. B. Neale, S. Levis, and D. A. Bailey, 2010: Improvements in a half degree atmosphere/land version of the CCSM. *Climate Dyn.*, **34**, 819–833, doi:10.1007/s00382-009-0614-8.

Gnanadesikan, A., 1999: A simple predictive model for the structure of the oceanic pycnocline. *Science*, **283**, 2077–2079, doi:10.1126/science.283.5410.2077.

——, M. Pradal, and R. Abernathey, 2015: Isopycnal mixing by mesoscale eddies significantly impacts oceanic anthropogenic carbon uptake. *Geophys. Res. Lett.*, **42**, 4249–4255, doi:10.1002/2015GL064100.

Gordon, A. L., 2001: Bottom water formation. *Encyclopedia of Ocean Sciences*, J. H. Steele, K. K. Turekian, and S. A. Thorpe, Eds., Academic Press, 334–340, doi:10.1006/rwos.2001.0006.

Gregory, J. M., 2000: Vertical heat transports in the ocean and their effect on time-dependent climate change. *Climate Dyn.*, **16**, 501–515, doi:10.1007/s003820000059.

Griffies, S. M., R. C. Pacanowski, and R. W. Hallberg, 2000: Spurious diapycnal mixing associated with advection in a *z*-coordinate ocean model. *Mon. Wea. Rev.*, **128**, 538–564, doi:10.1175/1520-0493(2000)128<0538:SDMAWA>2.0.CO;2.

——, and Coauthors, 2015: Impacts on ocean heat from transient mesoscale eddies in a hierarchy of climate models. *J. Climate*, **28**, 952–977, doi:10.1175/JCLI-D-14-00353.1.

Hallberg, R., and A. Gnanadesikan, 2006: The role of eddies in determining the structure and response of the wind-driven Southern Hemisphere overturning: Results from the Modeling Eddies in the Southern Ocean (MESO) project. *J. Phys. Oceanogr.*, **36**, 2232–2252, doi:10.1175/JPO2980.1.

Hansen, J., G. Russell, A. Lacis, I. Fung, and D. Rind, 1985: Climate response times: Dependence on climate sensitivity and ocean mixing. *Science*, **229**, 857–859, doi:10.1126/science.229.4716.857.

Held, I. M., M. Winton, K. Takahashi, T. Delworth, F. Zeng, and G. K. Vallis, 2010: Probing the fast and slow components of global warming by returning abruptly to preindustrial forcing. *J. Climate*, **23**, 2418–2427, doi:10.1175/2009JCLI3466.1.

Henning, C. C., and G. K. Vallis, 2005: The effects of mesoscale eddies on the stratification and transport of an ocean with a circumpolar channel. *J. Phys. Oceanogr.*, **35**, 880–896, doi:10.1175/JPO2727.1.

Heuzé, C., K. J. Heywood, D. P. Stevens, and J. K. Ridley, 2013: Southern Ocean bottom water characteristics in CMIP5 models. *Geophys. Res. Lett.*, **40**, 1409–1414, doi:10.1002/grl.50287.

Hill, C., D. Ferreira, J. M. Campin, J. Marshall, R. Abernathey, and N. Barrier, 2012: Controlling spurious diapycnal mixing in eddy-resolving height-coordinate ocean models—Insights from virtual deliberate tracer release experiments. *Ocean Modell.*, **45–46**, 14–26, doi:10.1016/j.ocemod.2011.12.001.

Ito, T., and J. Marshall, 2008: Control of lower-limb overturning circulation in the Southern Ocean by diapycnal mixing and mesoscale eddy transfer. *J. Phys. Oceanogr.*, **38**, 2832–2845, doi:10.1175/2008JPO3878.1.

Iudicone, D., G. Madec, and T. J. McDougall, 2008: Water-mass transformations in a neutral density framework and the key role of light penetration. *J. Phys. Oceanogr.*, **38**, 1357–1376, doi:10.1175/2007JPO3464.1.

Jacobs, S. S., 2004: Bottom water production and its links with the thermohaline circulation. *Antarct. Sci.*, **16**, 427–437, doi:10.1017/S095410200400224X.

Jayne, S. R., 2009: The impact of abyssal mixing parameterizations in an ocean general circulation model. *J. Phys. Oceanogr.*, **39**, 1756–1775, doi:10.1175/2009JPO4085.1.

Johnson, G. C., 2008: Quantifying Antarctic Bottom Water and North Atlantic Deep Water volumes. *J. Geophys. Res.*, **113**, C05027, doi:10.1029/2007JC004477.

Kirkman, C. H., IV, and C. M. Bitz, 2011: The effect of the sea ice freshwater flux on Southern Ocean temperatures in CCSM3: Deep-ocean warming and delayed surface warming. *J. Climate*, **24**, 2224–2237, doi:10.1175/2010JCLI3625.1.

Kirtman, B. P., and Coauthors, 2012: Impact of ocean model resolution on CCSM climate simulations. *Climate Dyn.*, **39**, 1303–1328, doi:10.1007/s00382-012-1500-3.

Kostov, Y., K. C. Armour, and J. Marshall, 2014: Impact of the Atlantic meridional overturning circulation on ocean heat storage and transient climate change. *Geophys. Res. Lett.*, **41**, 2108–2116, doi:10.1002/2013GL058998.

Kuhlbrodt, T., J. M. Gregory, and L. C. Shaffrey, 2015: A process-based analysis of ocean heat uptake in an AOGCM with an eddy-permitting ocean component. *Climate Dyn.*, **45**, 3205–3226, doi:10.1007/s00382-015-2534-0.

Levitus, S., J. I. Antonov, J. Wang, T. L. Delworth, K. W. Dixon, and A. J. Broccoli, 2001: Anthropogenic warming of Earth's climate system. *Science*, **292**, 267–270, doi:10.1126/science.1058154.

Lozier, M. S., 2010: Deconstructing the conveyor belt. *Science*, **328**, 1507–1511, doi:10.1126/science.1189250.

Marsh, R., A. J. G. Nurser, A. P. Megann, and A. L. New, 2000: Water mass transformation in the Southern Ocean of a global isopycnal coordinate GCM. *J. Phys. Oceanogr.*, **30**, 1013–1045, doi:10.1175/1520-0485(2000)030<1013:WMTITS>2.0.CO;2.

Marshall, J., K. C. Armour, J. R. Scott, Y. Kostov, U. Hausmann, D. Ferreira, T. G. Shepherd, and C. M. Bitz, 2014: The ocean's role in polar climate change: Asymmetric Arctic and Antarctic responses to greenhouse gas and ozone forcing. *Philos. Trans. Roy. Soc.*, **A372**, 20130040, doi:10.1098/rsta.2013.0040.

——, J. R. Scott, K. C. Armour, J.-M. Campin, M. Kelley, and A. Romanou, 2015: The ocean's role in the transient response of climate to abrupt greenhouse gas forcing. *Climate Dyn.*, **44**, 2287–2299, doi:10.1007/s00382-014-2308-0.

Maykut, G. A., 1982: Large-scale heat exchange and ice production in the central Arctic. *J. Geophys. Res.*, **87**, 7971, doi:10.1029/JC087iC10p07971.

McClean, J. L., and Coauthors, 2011: A prototype two-decade fully-coupled fine-resolution CCSM simulation. *Ocean Modell.*, **39**, 10–30, doi:10.1016/j.ocemod.2011.02.011.

Naveira Garabato, A. C., K. L. Polzin, B. A. King, K. J. Heywood, and M. Visbeck, 2004: Widespread intense turbulent mixing in the Southern Ocean. *Science*, **303**, 210–213, doi:10.1126/science.1090929.

——, D. P. Stevens, A. J. Watson, and W. Roether, 2007: Short-circuiting of the overturning circulation in the Antarctic

Circumpolar Current. *Nature*, **447**, 194–197, doi:10.1038/nature05832.

Nikurashin, M., and G. Vallis, 2011: A theory of deep stratification and overturning circulation in the ocean. *J. Phys. Oceanogr.*, **41**, 485–502, doi:10.1175/2010JPO4529.1.

——, and ——, 2012: A theory of the interhemispheric meridional overturning circulation and associated stratification. *J. Phys. Oceanogr.*, **42**, 1652–1667, doi:10.1175/JPO-D-11-0189.1.

——, ——, and A. Adcroft, 2012: Routes to energy dissipation for geostrophic flows in the Southern Ocean. *Nat. Geosci.*, **6**, 48–51, doi:10.1038/ngeo1657.

Orsi, A. H., G. C. Johnson, and J. L. Bullister, 1999: Circulation, mixing, and production of Antarctic Bottom Water. *Prog. Oceanogr.*, **43**, 55–109, doi:10.1016/S0079-6611(99)00004-X.

——, W. M. Smethie, and J. L. Bullister, 2002: On the total input of Antarctic waters to the deep ocean: A preliminary estimate from chlorofluorocarbon measurements. *J. Geophys. Res.*, **107**, 31-1–31-14, doi:10.1029/2001JC000976.

Pradal, M.-A., and A. Gnanadesikan, 2014: How does the Redi parameter for mesoscale mixing impact global climate in an Earth system model? *J. Adv. Model. Earth Syst.*, **6**, 586–601, doi:10.1002/2013MS000273.

Purkey, S. G., and G. C. Johnson, 2010: Warming of global abyssal and deep Southern Ocean waters between the 1990s and 2000s: Contributions to global heat and sea level rise budgets. *J. Climate*, **23**, 6336–6351, doi:10.1175/2010JCLI3682.1.

——, and ——, 2013: Antarctic Bottom Water warming and freshening: Contributions to sea level rise, ocean freshwater budgets, and global heat gain. *J. Climate*, **26**, 6105–6122, doi:10.1175/JCLI-D-12-00834.1.

Raper, S. C., J. M. Gregory, and R. J. Stouffer, 2002: The role of climate sensitivity and ocean heat uptake on AOGCM transient temperature response. *J. Climate*, **15**, 124–130, doi:10.1175/1520-0442(2002)015<0124:TROCSA>2.0.CO;2.

Redi, M., 1982: Oceanic isopycnal mixing by coordinate rotation. *J. Phys. Oceanogr.*, **12**, 1154–1158, doi:10.1175/1520-0485(1982)012<1154:OIMBCR>2.0.CO;2.

Rugenstein, M. A. A., M. Winton, R. J. Stouffer, S. M. Griffies, and R. Hallberg, 2013: Northern high-latitude heat budget decomposition and transient warming. *J. Climate*, **26**, 609–621, doi:10.1175/JCLI-D-11-00695.1.

Shakespeare, C. J., and A. McC. Hogg, 2012: An analytical model of the response of the meridional overturning circulation to changes in wind and buoyancy forcing. *J. Phys. Oceanogr.*, **42**, 1270–1287, doi:10.1175/JPO-D-11-0198.1.

Smith, R. D., M. E. Maltrud, F. O. Bryan, and M. W. Hecht, 2000: Numerical simulation of the North Atlantic Ocean at 1/10°. *J. Phys. Oceanogr.*, **30**, 1532–1561, doi:10.1175/1520-0485(2000)030<1532:NSOTNA>2.0.CO;2.

Snow, K., A. M. Hogg, S. M. Downes, B. M. Sloyan, M. L. Bates, and S. M. Griffies, 2015: Sensitivity of abyssal water masses to overflow parameterisations. *Ocean Modell.*, **89**, 84–103, doi:10.1016/j.ocemod.2015.03.004.

Speer, K., and E. Tziperman, 1992: Rates of water mass formation in the North Atlantic Ocean. *J. Phys. Oceanogr.*, **22**, 93–104, doi:10.1175/1520-0485(1992)022<0093:ROWMFI>2.0.CO;2.

Stewart, A. L., and A. F. Thompson, 2012: Sensitivity of the ocean's deep overturning circulation to easterly Antarctic winds. *Geophys. Res. Lett.*, **39**, L18604, doi:10.1029/2012GL053099.

——, and ——, 2013: Connecting Antarctic cross-slope exchange with Southern Ocean overturning. *J. Phys. Oceanogr.*, **43**, 1453–1471, doi:10.1175/JPO-D-12-0205.1.

——, and ——, 2015a: Eddy-mediated transport of warm Circumpolar Deep Water across the Antarctic shelf break. *Geophys. Res. Lett.*, **42**, 432–440, doi:10.1002/2014GL062281.

——, and ——, 2015b: The neutral density temporal residual mean overturning circulation. *Ocean Modell.*, **90**, 44–56, doi:10.1016/j.ocemod.2015.03.005.

——, R. Ferrari, and A. F. Thompson, 2014: On the importance of surface forcing in conceptual models of the deep ocean. *J. Phys. Oceanogr.*, **44**, 891–899, doi:10.1175/JPO-D-13-0206.1.

Stössel, A., M. M. Stössel, and J.-T. Kim, 2007: High-resolution sea ice in long-term global ocean GCM integrations. *Ocean Modell.*, **16**, 206–223, doi:10.1016/j.ocemod.2006.10.001.

Taylor, K. E., R. J. Stouffer, and G. A. Meehl, 2012: An overview of CMIP5 and the experiment design. *Bull. Amer. Meteor. Soc.*, **93**, 485–498, doi:10.1175/BAMS-D-11-00094.1.

Thompson, A. F., K. J. Heywood, S. Schmidtko, and A. L. Stewart, 2014: Eddy transport as a key component of the Antarctic overturning circulation. *Nat. Geosci.*, **7**, 879–884, doi:10.1038/ngeo2289.

Urakawa, L. S., and H. Hasumi, 2014: Effect of numerical diffusion on the water mass transformation in eddy-resolving models. *Ocean Modell.*, **74**, 22–35, doi:10.1016/j.ocemod.2013.11.003.

Walin, B. G., 1982: On the relation between sea-surface heat flow and thermal circulation in the ocean. *Tellus*, **34A**, 187–195, doi:10.1111/j.2153-3490.1982.tb01806.x.

Willmott, A. J., D. M. Holland, and M. A. Morales Maqueda, 2007: Polynya modelling. *Polynyas: Windows to the World*, W. O. Smith and D. G. Barber, Eds., Elsevier Oceanography Series, Vol. 74, Elsevier, 87–125, doi:10.1016/S0422-9894(06)74003-X.

Winton, M., K. Takahashi, and I. M. Held, 2010: Importance of ocean heat uptake efficacy to transient climate change. *J. Climate*, **23**, 2333–2344, doi:10.1175/2009JCLI3139.1.

——, W. G. Anderson, T. L. Delworth, S. M. Griffies, W. J. Hurlin, and A. Rosati, 2014: Has coarse ocean resolution biased simulations of transient climate sensitivity? *Geophys. Res. Lett.*, **41**, 8522–8529, doi:10.1002/2014GL061523.

Xie, P., and G. K. Vallis, 2012: The passive and active nature of ocean heat uptake in idealized climate change experiments. *Climate Dyn.*, **38**, 667–684, doi:10.1007/s00382-011-1063-8.

Zhang, Y., and G. K. Vallis, 2013: Ocean heat uptake in eddying and non-eddying ocean circulation models in a warming climate. *J. Phys. Oceanogr.*, **43**, 2211–2229, doi:10.1175/JPO-D-12-078.1.